MITSUBISHI ELECTRIC RESEARCH LABORATORIES
http://www.merl.com

Power Splitting-Based SWIPT with Decode-and-Forward Full-Duplex Relaying

Liu, H.; Kim, K.J.; Kwak, K.S.; Poor, H.V.

TR2016-141 August 2016

Abstract

This paper investigates simultaneous wireless information and power transfer (SWIPT) for a decode-and-forward (DF) full-duplex relay (FDR) network. A battery group consisting of two batteries is applied to utilize the relay-harvested energy for FDR transmission. The virtual harvest-use model and harvestuse-store model are considered, respectively. By switching between two batteries for charging and discharging with the aid of power splitting (PS), concurrent source and relay transmissions can overcome spectral efficiency loss compared to half-duplex relay (HDR)-assisted PS-SWIPT. The outage probability for the virtual harvest-use model is presented in an exact integral-form and the optimal PS (OPS) ratio that maximizes the end-to-end signal-to-interference-plus-noise ratio (e-SINR) is characterized in closed-form via the cubic formula. The fundamental tradeoff between the e-SINR and recycled self-power is quantified. The OPS ratios and corresponding outage probabilities in noiselimited and interference-limited environments are also derived. In the harvest-use-store model, a greedy switching (GS) policy is implemented with energy accumulation across transmission blocks. The OPS ratio of the GS policy is presented and the corresponding outage probability is derived by modeling the relays energy levels as a Markov chain with a two-stage state transition. Numerical results verify the performance improvement of the proposed scheme over HDR-assisted PS-SWIPT in terms of outage probability and average throughput.

IEEE Transactions on Wireless Communications

Power Splitting-Based SWIPT with Decode-and-Forward Full-Duplex Relaying

Hongwu Liu, *Member, IEEE,* Kyeong Jin Kim, *Senior Member, IEEE,*
Kyung Sup Kwak, *Member, IEEE,* and H. Vincent Poor *Fellow, IEEE*

***Abstract*—This paper investigates simultaneous wireless information and power transfer (SWIPT) for a decode-and-forward (DF) full-duplex relay (FDR) network. A battery group consisting of two batteries is applied to utilize the relay-harvested energy for FDR transmission. The virtual harvest-use model and harvest-use-store model are considered, respectively. By switching between two batteries for charging and discharging with the aid of power splitting (PS), concurrent source and relay transmissions can overcome spectral efficiency loss compared to half-duplex relay (HDR)-assisted PS-SWIPT. The outage probability for the virtual harvest-use model is presented in an exact integral-form and the optimal PS (OPS) ratio that maximizes the end-to-end signal-to-interference-plus-noise ratio (e-SINR) is characterized in closed-form via the cubic formula. The fundamental trade-off between the e-SINR and recycled self-power is quantified. The OPS ratios and corresponding outage probabilities in noise-limited and interference-limited environments are also derived. In the harvest-use-store model, a greedy switching (GS) policy is implemented with energy accumulation across transmission blocks. The OPS ratio of the GS policy is presented and the corresponding outage probability is derived by modeling the relay's energy levels as a Markov chain with a two-stage state transition. Numerical results verify the performance improvement of the proposed scheme over HDR-assisted PS-SWIPT in terms of outage probability and average throughput.**

***Index Terms*—Energy harvesting, wireless information and power transfer, decode-and-forward relay, full-duplex relay.**

I. Introduction

With the aid of energy harvesting (EH) from ambient radio-frequency (RF) signals, simultaneous wireless information and power transfer (SWIPT) becomes a promising supplemental technology for wireless communications [1]–[4]. By optimizing emitted and received RF signals, SWIPT, which benefits from controllable energy and information flows, can function under some extreme conditions, such as battle-field, underwater, and body area networks. Although the pioneering work on SWIPT has assumed extracting information and energy from the same received signal [1], [2], the door for SWIPT application has opened with the proposition of two types of separated receivers, namely, the time switching (TS) and power splitting (PS) architectures [3], [4]. In TS-based SWIPT (TS-SWIPT), the receiver harvests power from an energy signal sent by the source and then receives the source transmitted information signal in a time-division manner. In PS-based SWIPT (PS-SWIPT), the receiver extracts energy from the received source signal with the aid of PS. Generally, PS-SWIPT reduces the timeslots consumed compared with TS-SWIPT, so that the information transmission time, as well as the spectral efficiency, can be increased. The applications of TS-SWIPT and PS-SWIPT have been considered in various wireless systems, such as multiple-input multiple-output (MIMO) systems [4], orthogonal frequency division multiplexing systems [5], cognitive systems [6], and cellular systems [7], [8].

One line of research that has recently emerged is relay-assisted SWIPT, which not only keeps energy-constrained relay nodes active through RF EH, but also takes advantage of an information-energy tradeoff. The study in [9] proposes two SWIPT mechanisms for amplify-and-forward (AF) relay networks: PS-SWIPT and TS-SWIPT relaying protocols. For decode-and-forward (DF) relay networks, the throughputs of PS-SWIPT and TS-SWIPT relaying protocols have been investigated in [10]. When a single relay is deployed, power allocation for EH relay-assisted multiple transceiver pairs was studied in [11]. The outage and diversity of relay-assisted SWIPT have been investigated in [12] when multiple relays are distributed with spatial randomness. For relay networks where interference cannot be ignored, [13] has investigated a distributed PS-SWIPT and [14] has proposed to apply multiple antennas at the relay to suppress interference. Moreover, smart antenna technologies, including antenna switching and antenna selection, have been applied for relay-assisted SWIPT networks [15]–[17].

All the above mentioned studies for relay-assisted SWIPT are restricted to a half-duplex relay (HDR) at the price of 50% loss in spectral efficiency since two time slots are required to transmit one data packet. Full-duplex transmission, which was previously regarded as impractical due to strong self-interference (SI), has regained considerable interest from both academia and industry in developing future Wireless Local Area Networks (WLANs) [18], WiFi networks [19], and 5G networks [20]. Of particular interest is when SI can be

H. Liu is with Shandong Jiaotong University, Jinan, China (e-mail: hong.w.liu@hotmail.com).

K. J. Kim is with Mitsubishi Electric Research Laboratories, Cambridge, MA (e-mail: kyeong.j.kim@hotmail.com).

K. S. Kwak is with Tellab, Inha University, Incheon, Korea (e-mail: kskwak@inha.ac.kr).

H. V. Poor is with Department of Electrical Engineering, Princeton University, Princeton, NJ (e-mail: poor@princeton.edu).

This work was supported by SRF for ROCS, SEM, Shandong Provincial Natural Science Foundation, China (2014ZRB019XM). This work was supported in part by the MSIP (Ministry of Science, ICT and Future Planning), Korea, under the ITRC (Information Technology Research Center) support program (IITP-2016-H8501-16-1019) supervised by the IITP (Institute for Information & communications Technology Promotion) and by National Research Foundation of Korea-Grant funded by the Korean Government (Ministry of Science, ICT and Future Planning)-NRF-2014K1A3A1A20034987). This work was supported in part by the U. S. National Science Foundation under Grant ECCS-1343210.

significantly suppressed, the implementation of a full-duplex relay (FDR) can overcome the spectral efficiency loss of HDR. In standards developments, the use of FDR networks has also been proposed for 3GPP Long-Term Evolution (LTE) [21] and Worldwide Interoperability for Microwave Access (WiMAX) systems [22]. With recent advances in SI cancellation technologies, studies have shown that 70-100 dB overall attenuation levels of SI can be achieved [23], [24]. However, SI cannot be eliminated completely because of RF impairments [25], so that the performance of FDR networks is still limited by residual SI (RSI) and several approaches have been proposed to optimize the performance of FDR networks, including relay power control [26]–[28], spatial-domain processing [29], and relay selection [30], [31]. For AF and DF FDR networks, the performance of relay-assisted TS-SWIPT has been studied in [32]. Moreover, multiple transmit/receive antennas have been employed at the relay to enhance the performance of TS-SWIPT in DF FDR networks [33]. When TS-SWIPT is deployed in FDR networks [32], [33], each transmission cycle T is divided into two phases by a TS factor $\kappa \in (0,1)$, so that the source-to-relay link is used for relay EH in the first phase with a duration of κT and the relay-assisted information transmission is conducted in the second phase with a duration of $(1-\kappa)T$. By dividing each transmission cycle equally into two time phases, [34] proposed another type of full-duplex TS-SWIPT by employing relay transmission and relay self-energy recycling simultaneously in the second half time phase. Unfortunately, all the aforementioned TS-SWIPT schemes are not strictly operated in FDR mode due to TS implementation, so that the spectral efficiency loss is unavoidable. On the other hand, PS-SWIPT has shown its performance improvement over TS-SWIPT in both point-to-point transmissions [3], [4] and HDR networks [9], [10]. Since PS operation does not change the effective information transmission time in relay networks [9], [10], PS-SWIPT has the potential to fully exploit FDR, so that the effective information transmission time can be doubled compared to that of HDR networks.

To the best of our knowledge, PS-SWIPT has not been applied in FDR networks. As an attempt to improve relaying efficiency of an FDR network with SWIPT, this paper proposes a DF FDR-assisted PS-SWIPT scheme, which allows a DF relay to simultaneously transmit and receive signals at the same time, leading to truly full-duplex information transfer.

The main contributions of this paper include: (i) We propose to periodically switch between two rechargeable batteries for charging and discharging during two consecutive time slots of each block, so that the energy-constrained relay can be self-powered in a virtual harvest-use model. The fundamental trade-off between the end-to-end signal-to-interference-plus-noise ratio (SINR) and recycled self-power is quantified. We derive an exact integral-form expression for the end-to-end outage probability and validate this via simulation. We characterize the optimal PS (OPS) ratio that maximizes the end-to-end SINR (e-SINR) by solving a cubic equation, which has a closed-form solution. (ii) For the PS-SWIPT scheme with a fixed PS ratio, we derive the end-to-end outage probabilities of the considered DF FDR network in noise-limited and interference-limited environments, respectively. Additionally, the closed-form OPS ratios in noise-limited and interference-limited environments are respectively presented and analytical expressions for the corresponding outage probabilities are derived. It is shown for the first time that the RSI in the RF-domain is beneficial in decreasing the end-to-end outage probability of the DF FDR network with PS-SWIPT, so that the interference cancellation (IC) burden in the RF-domain can be alleviated. (iii) To utilize the relay-harvested energy efficiently in case of deep fading channels, in which the successful EH and information relaying cannot be guaranteed, we also propose a harvest-use-store model for FDR-assisted PS-SWIPT with a greedy switching (GS) implementation. The OPS ratio of the GS policy and the corresponding outage probability are derived. Numerical results verify the improved system performance of the GS policy over the virtual harvest-use model in the scenario of weak EH quality.

The rest of this paper is organized as follows. Section II describes the system model and the virtual harvest-use model of the considered DF FDR-assisted PS-SWIPT. The analytical results of the virtual harvest-use model are also presented in Section II. Section III presents the harvest-use-store model and its GS implementation. Section IV presents numerical results and discusses the system performance of our proposed scheme. Finally, Section V summarizes the contributions of this study.

Notation: $\lfloor\cdot\rfloor$ is the floor function, $f_{\varphi}(\cdot)$, $F_{\varphi}(\cdot)$, and $\bar{F}_{\varphi}(\cdot)$ denote the probability density function (PDF), the cumulative distribution function (CDF) and the complementary CDF (CCDF) of the random variable (RV) φ, respectively, $\mathbb{E}\{\cdot\}$ denotes expectation, $\mathbb{R}^{M\times N}$ denotes the $M \times N$ dimensional real space, $K_n(\cdot)$ is the n-th order modified Bessel function of the second kind [35, Eq. 8.432], and $Q_1(\cdot,\cdot)$ is the first-order Marcum Q-function [36, Eq. 4.33].

II. PS-SWIPT of Virtual Harvest-Use Model

A. System Model

In the considered DF FDR network, a source intends to transmit its information to a destination. Due to physical isolation between the source and destination, a DF relay operating in FDR mode is employed to relay the source information to the destination. The relay is assumed to be energy-constrained such that it has to harvest energy from the received RF signals to forward the information. For simplicity of implementation, the source and destination are each equipped with a single antenna, whereas the relay is equipped with two separated antennas for receiving and transmitting, respectively.

The channels of the source-to-relay and relay-to-destination links are denoted by $h_1 = \sqrt{\mathcal{L}_1}\tilde{h}_1$ and $h_2 = \sqrt{\mathcal{L}_2}\tilde{h}_2$, respectively, where $\mathcal{L}_i$ and $\tilde{h}_i$ $(i = 1, 2)$ are the large-scale path-loss and small-scale fading of dual-hop links, respectively. The large-scale path-loss is modeled as $\mathcal{L}_i = \frac{\mathcal{A}_i\mathcal{L}}{(d_i/d_0)^{\varphi}}$ $(i = 1, 2)$, where φ is the path loss exponent, d_0 is the reference distance, d_i is the distance between the transmitter and receiver of the channel h_i, $\mathcal{L}$ is the measured path loss at d_0, and $\mathcal{A}_i$ denotes the transmit antenna gain. For the sake of exposition, the channel gain and average channel gain of h_i are denoted by $g_i \triangleq |h_i|^2$ and $\bar{g}_i \triangleq \mathbb{E}\{|h_i|^2\}$ for $i \in \{1, 2, a, b\}$, respectively. The small-scale channel magnitude, $|\tilde{h}_i|$ $(i = 1, 2)$, is modeled

as Nakagami-m fading with the unit mean such that g_i $(i = 1, 2)$ is distributed according to the gamma distribution with the shape factor m_i and the scale factor $\theta_i \triangleq \frac{\bar{g}_i}{m_i}$. Then, the PDF, CDF, and CCDF of g_i $(i = 1, 2)$ can be respectively expressed as

$$f_{g_i}(x) = \frac{1}{\Gamma(m_i)\theta_1^{m_i}} x^{m_i-1} e^{-x/\theta_i}, \tag{1}$$

$$F_{g_i}(x) = 1 - \frac{\Gamma_u(m_i, x/\theta_i)}{\Gamma(m_i)}, \text{ and } \bar{F}_{g_i}(x) = \frac{\Gamma_u(m_i, x/\theta_i)}{\Gamma(m_i)}. \tag{2}$$

The above fading assumption is fairly general and allows us to characterize a wide range of channel models including both line-of-sight and non-line-of-sight links. At the relay, the RSI channels incident on the receive antenna and observed in the baseband after IC processing are denoted by h_a and h_b, respectively. Notably, the harvested energy at the relay is partially determined by h_a, whereas the decoding performance of the relay is affected by h_b. Based on the experimental results of [24], the RSI channel observed in the RF-domain before any active IC is modeled as Rician. To the best of the authors' knowledge, the distribution of h_b, i.e., the RSI channel in the digital-domain, is not known in practice due to the complicated processing of several different stages of IC [28], [37] . Based on the recent advance of optimal training in channel state information (CSI) estimation for energy-constrained networks [38], we assume that the relay can access perfect CSI in this study.

The proposed virtual harvest-use model deploys a battery group consisting of two rechargeable batteries, as depicted in Fig. 1. Without loss of generality, we assume that each battery contains enough redundant energy initially. All channels are assumed to be quasi-static and the channel coefficients are constant for one block but vary independently at a block level. By denoting the duration of each block by T, each block is divided equally into two time slots, i.e., the odd and even slots with the same duration $\frac{T}{2}$. The two batteries are activated for EH and power supplying in a time-switching manner, i.e., in the odd (even) slot of a block, the relay transmission power is supplied by battery #1 (battery #2), while the relay-harvested energy during the odd (even) slot is stored in battery #2 (battery #1). In each block, we also assume that the consumed energy quantum of battery #1 (battery #2) in the odd (even) slot equals to that of the relay-harvested energy during the even (odd) slot. Since this charging/discharging implementation mimics the harvest-use model of HDR PS-SWIPT [9], [10], where a single energy storage unit is applied, we call it the virtual harvest-use model, which can power the relay transmission in a self-sustainable way.

In each time slot, the power of the relay-received signal is split for EH and information detecting (ID) according to the proportion $\rho : 1 - \rho$, where $\rho \in (0, 1)$ is the PS ratio. Due to a negligible power of additive Gaussian noise at the relay receive antenna, the input signal at the EH receiver can be written as

$$y_{eh}(t) = \sqrt{\rho}\left(\sqrt{p_s} h_1 s(t) + \sqrt{p_r} h_a \tilde{s}(t)\right), \tag{3}$$

where p_s is the source transmission power, p_r is the relay transmission power, $s(t)$ is the normalized source signal

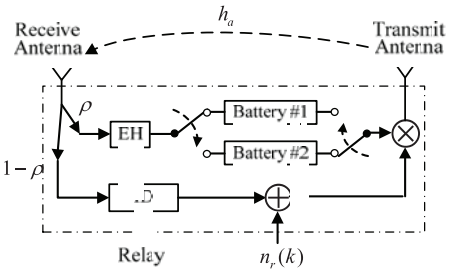

Fig. 1. Block diagram of the considered FDR node.

satisfying $\mathbb{E}\{|s(t)|^2\} = 1$, and $\tilde{s}(t)$ is the relay transmit signal satisfying $\mathbb{E}\{|\tilde{s}(t)|^2\} = 1$. For sake of fairly comparison between the proposed scheme and the HDR transmission, in the t-th block, we denote that $s(t) = s_o(t)$ for the odd slot, $s(t) = s_e(t)$ for the even slot, and $s_o(t) \neq s_e(t)$. Note that $y_{eh}(t)$ will be sent to battery #2 (battery #1) for charging in the odd (even) slot. At the end of a time slot, the relay-harvested energy can be expressed as

$$E_h = \eta_h \rho \left(p_s g_1 + p_r g_a\right) \tfrac{T}{2}, \tag{4}$$

where η_h $(0 < \eta_h < 1)$ is the energy conversion efficiency with respect to RF-to-DC and battery charging. Simultaneously, the relay transmission in the current slot is powered by the battery that is not switched for EH. By using E_h as the transmission energy quantum, the relay transmission power is characterized by

$$p_r = \frac{\eta_t E_h}{T/2} \triangleq \eta\rho\left(p_s g_1 + p_r g_a\right) \triangleq \eta(\tilde{p}_s + p_{\text{rsi}}) \tag{5}$$

where η_t $(0 < \eta_t < 1)$ is the utilizing efficiency with respect to the battery discharging, $\eta \triangleq \eta_t \eta_h$, $\tilde{p}_s \triangleq \rho p_s g_1$, and $p_{\text{rsi}} \triangleq \rho p_r g_a$ denotes the available self-power due to EH from RSI. Although the recycled self-power can be utilized, a successful relay-destination transmission cannot be guaranteed by solely recycling the self-power. From (4) and (5), it can be shown that the term $\tilde{p}_s$ is the only external energy source for EH. To ensure that the relay can harvest enough energy for transmission, a piecewise behavior is assumed in the harvest-use model, i.e., the EH and ID receivers are activated only when

$$\tilde{p}_s > S_{\min}, \tag{6}$$

where $S_{\min}$ is the EH receiver sensitively [39]. Without loss of generality, we normalize the slot duration by $\frac{T}{2} = 1$ and equivalently use energy and power in the following presentation. Based on (5), the relay transmission power given that (6) holds can be expressed as

$$p_r = \frac{\eta\rho p_s g_1}{1 - \eta\rho g_a}. \tag{7}$$

In practice, g_a is less than 1 due to passive IC such as antenna isolation, so that the denominator of p_r in (7) is positive. With the DF protocol, the relay first decodes the original source signal and then regenerates the signal [40]. Hence, the relay transmit signal can be expressed as $\tilde{s}(t) = s(t - \tau)$ by assuming the correct decoding of the source signal, where τ is the processing delay at the relay. Noticing the relay

transmission power in (7), the sampled received signal after active IC at the relay can be expressed as

$$\begin{aligned} y_r(k) &= \sqrt{(1-\rho)p_s}h_1 s(k) + \sqrt{(1-\rho)p_r}h_b\tilde{s}(k) + n_r(k) \\ &= \sqrt{(1-\rho)p_s}h_1 s(k) + \sqrt{\tfrac{(1-\rho)\eta\rho p_s g_1}{1-\eta\rho g_a}}h_b s(k-\tau) \\ &\quad + n_r(k), \end{aligned} \tag{8}$$

where k denotes the symbol index, $s(k)$ and $\tilde{s}(k)$ are the sampled signals of $s(t)$ and $\tilde{s}(t)$, respectively, and $n_r(k) \triangleq \sqrt{1-\rho}n_a(k) + n_p(k)$ is the equivalent sampled noise with the sampled receive antenna noise $n_a(k)$ and the sampled processing noise $n_p(k)$. The statistically independent noises $n_a(k)$ and $n_p(k)$ have zero means and variances σ_a^2 and σ_p^2, respectively. Since $n_r(k)$ is dominated by the processing noise instead of the negligible antenna noise [3], $n_r(k)$ can be approximated as having zero mean and variance $\sigma_r^2 \approx \sigma_p^2$. Based on (8), the SINR at the relay can be expressed as

$$\gamma_r = \frac{(1-\rho)p_s g_1}{\frac{(1-\rho)\eta\rho p_s g_1 g_b}{1-\eta\rho g_a} + \sigma_r^2}. \tag{9}$$

At the destination, the sampled received signal is given by

$$\begin{aligned} y_d(k) &= \sqrt{p_r}h_2 s(k-\tau) + n_d(k) \\ &= \sqrt{\tfrac{\eta\rho p_s g_1}{1-\eta\rho g_a}}h_2 s(k-\tau) + n_d(k), \end{aligned} \tag{10}$$

where $n_d(k)$ is the additive noise at the destination with zero mean and variance σ_d^2. Based on (10), the SINR at the destination can be evaluated as

$$\gamma_d = \frac{\eta\rho p_s g_1 g_2}{(1-\eta\rho g_a)\sigma_d^2}. \tag{11}$$

Then, the e-SINR can be expressed as $\gamma = \min\{\gamma_r, \gamma_d\}$.

B. Optimal PS and Outage Probability Analysis

In this section, the OPS is proposed as a way of enhancing the end-to-end system performance. We begin by formulating the OPS ratio optimization problem and analyzing the outage probability of the investigated DF FDR network. Then, we present the OPS ratios to achieve the allowed maximum e-SINR in noise-limited and interference-limited environments, respectively.

The OPS ratio $\tilde{\rho}^*$ that minimizes the end-to-end outage probability can be obtained by solving the following optimization problem:

$$\begin{aligned} &\tilde{\rho}^* = \arg\min_{\rho} P_{\text{out}}^{\text{FDR}}, \\ &\text{s.t.} \;\; 0 < \rho < 1, \end{aligned} \tag{12}$$

where $P_{\text{out}}^{\text{FDR}} \triangleq \Pr\{(\tilde{p}_s \le S_{\min}) \cup ((\tilde{p}_s > S_{\min}) \cap (\gamma < \gamma_{\text{th}}))\}$ is the end-to-end outage probability of the DF FDR network and γ_{th} is an SINR threshold for correct data detection at the destination. Note that both the EH outage and information transmission outage have been considered in (12). In order to reveal the effect of the RSI on the performance of the investigated DF FDR network, we have assumed that h_a and h_b stand for the RSI channels observed in the RF-domain (before active IC) and digital-domain (after active IC), respectively, so that the term p_{rsi} in (5) can accurately represent the available self-power due to RSI. The incident RSI on the relay receive antenna can be further suppressed by the active IC techniques [23], [24], [41], which makes the ID receiver suffer a lower RSI, i.e., $\sqrt{(1-\rho)p_r}h_b s(k-\tau)$ in (8), where $0 < |h_b| \le |h_a|$ and $|h_b| = |h_a|$ denotes that the active IC has not been applied to the sampled signal. Nevertheless, due to the complicated processing of different stages in active IC, the distribution of the RSI in the digital-domain is not known in practice, whereas the RSI channel power can be characterized according to the signal model of (8). In the follows, we investigate the system performance of the DF FDR network and derive the end-to-end outage probability conditioned on the RSI channel power in the digital-domain.

Proposition 1. *Conditioned on g_b, the end-to-end outage probability achieved by PS-SWIPT in the DF FDR network is given by*

$$P_{\text{out}}^{\text{FDR}} = 1 - I_1 I_2, \tag{13}$$

where

$$I_1 \triangleq \begin{cases} \bar{F}_{g_1}(\alpha_1) - \tilde{I}_1(\alpha_1), & g_b \le \frac{1-\eta\rho}{\eta\rho\gamma_{\text{th}}} \text{ and } \alpha_3 \le \alpha_1 \\ \bar{F}_{g_1}(\alpha_3) - \tilde{I}_1(\alpha_3), & g_b \le \frac{1-\eta\rho}{\eta\rho\gamma_{\text{th}}} \text{ and } \alpha_1 < \alpha_3 \le \alpha_2 \\ \bar{F}_{g_1}(\alpha_3), & g_b \le \frac{1-\eta\rho}{\eta\rho\gamma_{\text{th}}} \text{ and } \alpha_3 > \alpha_2 \\ \bar{F}_{g_1}(\alpha_1) - \tilde{I}_2(\alpha_1), & \frac{1-\eta\rho}{\eta\rho\gamma_{\text{th}}} < g_b \le \frac{1}{\eta\rho(\gamma_{\text{th}}+1)} \text{ and } \alpha_3 \le \alpha_1 \\ \bar{F}_{g_1}(\alpha_3) - \tilde{I}_2(\alpha_3), & \frac{1-\eta\rho}{\eta\rho\gamma_{\text{th}}} < g_b \le \frac{1}{\eta\rho(\gamma_{\text{th}}+1)} \text{ and } \alpha_3 > \alpha_1 \\ 0, & g_b > \frac{1}{\eta\rho(\gamma_{\text{th}}+1)} \end{cases}, \tag{14a}$$

$$I_2 \triangleq \bar{F}_y(\beta) - \tilde{I}_3, \tag{14b}$$

$$\tilde{I}_1(\alpha) \triangleq \frac{1}{\Gamma(m_1)\theta_1^{m_1}} \int_{\alpha}^{\alpha_2} x^{m_1-1} e^{-x/\theta_1} \bar{F}_{g_a}(z_1(x)) \mathrm{d}x, \tag{14c}$$

$$\tilde{I}_2(\alpha) \triangleq \frac{1}{\Gamma(m_1)\theta_1^{m_1}} \int_{\alpha}^{\infty} x^{m_1-1} e^{-x/\theta_1} \bar{F}_{g_a}(z_1(x)) \mathrm{d}x, \tag{14d}$$

$$\begin{aligned} \tilde{I}_3 \triangleq \frac{2}{\Gamma(m_1)\Gamma(m_2)} &\int_{(1-\eta\rho)\beta}^{(1-\eta\rho g_b)\beta} y^{\frac{1}{2}m_1 + \frac{1}{2}m_2 - 1} \\ &\times K_{m_1-m_2}(2\sqrt{y}) F_{g_a}(z_2(y)) \mathrm{d}y, \end{aligned} \tag{14e}$$

$\alpha_1 \triangleq \frac{(1-\eta\rho g_b)\gamma_{\text{th}}\sigma_r^2}{(1-\rho)(1-\eta\rho g_b(\gamma_{\text{th}}+1))p_s}$, $\alpha_2 \triangleq \frac{(1-\eta\rho)\gamma_{\text{th}}\sigma_r^2}{(1-\rho)(1-\eta\rho(g_b\gamma_{\text{th}}+1))p_s}$, $\alpha_3 \triangleq \frac{S_{\min}}{\rho p_s}$, $\beta \triangleq \frac{\gamma_{\text{th}}\sigma_d^2}{\eta\rho p_s\theta_1\theta_2}$, $z_1(x) \triangleq \frac{1}{\eta\rho} - \frac{(1-\rho)p_s g_b \gamma_{\text{th}} x}{(1-\rho)p_s x - \gamma_{\text{th}}\sigma_r^2}$, $z_2(y) \triangleq \frac{1}{\eta\rho} - \frac{p_s\theta_1\theta_2 y}{\gamma_{\text{th}}\sigma_d^2}$, *$F_{g_a}(x)$ and $\bar{F}_{g_a}(x)$ are the CDF and CCDF of the truncated RV $g_a \in [g_b, 1)$, respectively,* $\bar{F}_y(y) = 1 - \frac{2^{2-m_1-m_2}}{\Gamma(m_1)\Gamma(m_2)} D_{m_1+m_2-1, m_1-m_2}(2\sqrt{y})$ *is the CCDF of $y \triangleq \frac{g_1 g_2}{\theta_1\theta_2}$, and $D_{\mu,\nu}(y) = \int_0^y x^{\mu} K_{\nu}(x)\mathrm{d}x$.*

Proof. See Appendix A. □

Remark 1: Proposition 1 explicitly shows that when $g_b > \frac{1}{\eta\rho(\gamma_{\text{th}}+1)}$, $P_{\text{out}}^{\text{FDR}} = 1$. Thus, a successful end-to-end transmission requires eliminating the RSI in the baseband at least by $g_b < \frac{1}{\eta\rho(\gamma_{\text{th}}+1)}$. The numerical evaluation of the integral-form expressions in I_1 and I_2 can be rapidly performed using computational software such as Mathematica and Matlab.

Due to the complicated expression of (13), a closed-form solution of (12) can hardly be obtained. However, when $\tilde{p}_s > S_{\min}$ is satisfied, we are interested in finding the OPS ratio that

maximizes the e-SINR, which is the solution of the following optimization problem:

$$\rho^* = \arg\max_{\rho} \ \gamma, \quad \text{s.t.} \ \ 0 < \rho < 1. \tag{15}$$

By sequentially substituting (5) into in (9), (11), and $\gamma = \min(\gamma_r, \gamma_d)$ in solving for $p_{\rm rsi}$, the trade-off between the RSI-determined self-power and the e-SINR can be expressed as

$$p_{\rm rsi} = \begin{cases} \frac{1}{\eta g_b}\left(\frac{p_s g_1}{\gamma} - \frac{\sigma_r^2}{1-\rho}\right) - \rho p_s g_1, & \gamma_r < \gamma_d \\ \frac{\gamma \sigma_d^2}{\eta g_2} - \rho p_s g_1, & \gamma_r \geq \gamma_d \end{cases}. \tag{16}$$

Remark 2: The trade-off in (16) implies that when $\gamma_r < \gamma_d$, an increasing e-SINR requires decreasing $p_{\rm rsi}$, while when $\gamma_r \geq \gamma_d$, an increasing $p_{\rm rsi}$ leads to an increasing e-SINR. This result shows that when the e-SINR is limited by the first-hop link (second-hop link), g_a is detrimental (beneficial) in increasing the e-SINR. Hence, to obtain an e-SINR as high as possible, it needs decreasing (increasing) g_a when $\gamma_r < \gamma_d$ ($\gamma_r \geq \gamma_d$). Further, (16) explicitly shows that the eliminating for the RSI in the baseband as much as possible is beneficial in increasing γ when $\gamma_r < \gamma_d$. When $\gamma_r \geq \gamma_d$, (16) shows that eliminating g_b is not necessary. Nevertheless, the correct decoding at the relay still relies on g_b, i.e., $g_b < \frac{1}{\eta\rho(\gamma_{\rm th}+1)}$, as presented in Proposition 1.

Proposition 2. *The OPS ratio ρ^* that maximizes the e-SINR of the DF FDR network is given by*

$$\rho^* = \begin{cases} \textit{the 1st root of } C(\rho) = 0, & \frac{g_a^2}{g_b} > \frac{p_s g_1 g_2}{\sigma_d^2} \\ \textit{the 2nd root of } C(\rho) = 0, & \frac{g_a^2}{g_b} < \frac{p_s g_1 g_2}{\sigma_d^2} \end{cases}, \tag{17}$$

where $C(\rho) \triangleq a_3\rho^3 + a_2\rho^2 + a_1\rho + a_0$ is a cubic polynomial, $a_0 = -\sigma_d^2$, $a_1 = \eta(g_2\sigma_r^2 + 2g_a\sigma_d^2) + \sigma_d^2$, $a_2 = \eta^2 g_2(p_s g_1 g_b - g_a\sigma_r^2) - (1+\eta g_a)^2\sigma_d^2 + \sigma_d^2$, and $a_3 = \eta^2(g_a^2\sigma_d^2 - p_s g_1 g_2 g_b)$.

Proof. See Appendix B. □

Noticing that a closed-form solution known as the cubic formula exists for the solution of an arbitrary cubic equation [42], the closed-form ρ^* in Proposition 2 is obtained by solving the cubic function $C(\rho) = 0$. Since the roots of this cubic function are extremely complicated and lengthy, we have omitted their closed-form expressions due to the space limitations. Nevertheless, the numerical value of ρ^* can be easily obtained by programming Ferrari's method [42].

Proposition 3. *When the source transmission power goes to infinity, the performance floor of the end-to-end outage probability achieved by PS-SWIPT in the DF FDR network is given by*

$$P_{\rm out}^{\infty} = 1 - I_1^{\infty}, \tag{18}$$

where

$$I_1^{\infty} = \begin{cases} 1, & g_b \leq \frac{1-\eta\rho}{\eta\rho\gamma_{\rm th}} \\ F_{g_a}\left(\frac{1}{\eta\rho} - g_b\gamma_{\rm th}\right), & \frac{1-\eta\rho}{\eta\rho\gamma_{\rm th}} < g_b \leq \frac{1}{\eta\rho(\gamma_{\rm th}+1)} \\ 0, & g_b > \frac{1}{\eta\rho(\gamma_{\rm th}+1)} \end{cases}. \tag{19}$$

Proof. See Appendix C. □

Remark 3: Proposition 3 explicitly shows that in the high signal-to-noise condition, the performance floor of the proposed scheme is determined by the RSI instead of the CSI of dual-hop links. Further, when $g_b \leq \frac{1-\eta\rho}{\eta\rho\gamma_{\rm th}}$, we have $P_{\rm out}^{\infty} \to 0$; whereas when $g_b > \frac{1}{\eta\rho(\gamma_{\rm th}+1)}$, an outage occurs with the probability 1.

C. OPS in Noise-limited Environment

With respect to the RSI at the relay, considerable interference isolation can be achieved by separating the antennas and employing IC [24], [41]. In addition, the receiver and processing noises are much greater than the background thermal noise in SWIPT systems [3], [4]. Therefore, it is reasonable to assume a noise-limited environment in the considered DF FDR network.

In the noise-limited environment, the RSI is negligible. The SINRs at the relay and destination are respectively approximated as

$$\gamma_r \approx \frac{(1-\rho)p_s g_1}{\sigma_r^2} \ \ \text{and} \ \ \gamma_d \approx \frac{\eta\rho p_s g_1 g_2}{\sigma_d^2}. \tag{20}$$

Proposition 4. *In the noise-limited environment, the end-to-end outage probability achieved by PS-SWIPT in the DF FDR network is given by*

$$P_{\rm out}^{\rm N} = 1 - \bar{F}_y\left(\frac{\sigma_d^2\gamma_{\rm th}}{\eta\rho p_s\theta_1\theta_2}\right) I_1^{\rm N}, \tag{21}$$

where $\bar{F}_y(y) = 1 - \frac{2^{2-m_1-m_2}}{\Gamma(m_1)\Gamma(m_2)} D_{m_1+m_2-1, m_1-m_2}(2\sqrt{y})$, $D_{\mu,\nu}(y) = \int_0^y x^{\mu} K_{\nu}(x)\mathrm{d}x$, and $I_1^{\rm N}$ is given by

$$I_1^{\rm N} = \begin{cases} \bar{F}_{g_1}\left(\frac{S_{\min}}{\rho p_s}\right), & \gamma_{\rm th} < \frac{(1-\rho)S_{\min}}{\rho\sigma_r^2} \\ \bar{F}_{g_1}\left(\frac{\sigma_r^2\gamma_{\rm th}}{(1-\rho)p_s}\right), & \gamma_{\rm th} \geq \frac{(1-\rho)S_{\min}}{\rho\sigma_r^2} \end{cases}. \tag{22}$$

Proof. In the noise-limited environment, we have

$$\begin{aligned} I_1^{\rm N} &\triangleq \Pr\{(\tilde{p}_s > S_{\min}) \cap (\gamma_r > \gamma_{\rm th})\} \\ &= \Pr\left\{\left(g_1 > \tfrac{S_{\min}}{\rho p_s}\right) \cap \left(g_1 > \tfrac{\sigma_r^2\gamma_{\rm th}}{(1-\rho)p_s}\right)\right\} \end{aligned} \tag{23}$$

and

$$I_2^{\rm N} \triangleq \Pr(\gamma_d > \gamma_{\rm th}) = \Pr\left(\left(y > \tfrac{\sigma_d^2\gamma_{\rm th}}{\eta\rho p_s\theta_1\theta_2}\right)\right), \tag{24}$$

respectively, where $y \triangleq \frac{g_1 g_2}{\theta_1\theta_2}$. Noticing that the CCDFs of g_1 and y are respectively given by $\bar{F}_{g_1}(x) = \frac{\Gamma_u(m_1, x/\theta_1)}{\Gamma(m_1)}$ and $\bar{F}_y(y) = 1 - \frac{2^{2-m_1-m_2}}{\Gamma(m_1)\Gamma(m_2)} D_{m_1+m_2-1, m_1-m_2}(2\sqrt{y})$ and following the similar procedure of (A.2), we can express the end-to-end outage probability as (21). □

Proposition 5. *In the noise-limited environment, the OPS ratio ρ^* that maximizes the e-SINR is given by*

$$\rho^* = \frac{\sigma_d^2}{\sigma_d^2 + \eta g_2\sigma_r^2}, \tag{25}$$

and the corresponding end-to-end outage probability is given by

$$P_{\rm out}^{\rm N^*} = I_3^{\rm N} + I_4^{\rm N}, \tag{26}$$

where

$$I_3^{\mathrm{N}} = F_{g_1}\left(\frac{\gamma_{\mathrm{th}}\sigma_r^2}{p_s}\right) + \int_{\alpha}^{\frac{\gamma_{\mathrm{th}}\sigma_r^2+S_{\min}}{p_s}} f_{g_1}(x) F_{g_2}\left(\frac{(p_s x - S_{\min})\sigma_d^2}{\eta S_{\min}\sigma_r^2}\right) \mathrm{d}x + \int_{\frac{\gamma_{\mathrm{th}}\sigma_r^2+S_{\min}}{p_s}}^{\infty} f_{g_1}(x) F_{g_2}\left(\frac{\gamma_{\mathrm{th}}\sigma_d^2}{\eta(p_s x - \gamma_{\mathrm{th}}\sigma_r^2)}\right) \mathrm{d}x, \quad (27)$$

$$I_4^{\mathrm{N}} = 1 - \int_{\frac{S_{\min}}{p_s}}^{\infty} f_{g_1}(x) F_{g_2}\left(\frac{(p_s x - S_{\min})\sigma_d^2}{\eta S_{\min}\sigma_r^2}\right) \mathrm{d}x, \quad (28)$$

and $\alpha = \begin{cases} \frac{S_{\min}}{p_s}, & \gamma_{\mathrm{th}} \le \frac{S_{\min}}{\sigma_r^2} \\ \frac{\gamma_{\mathrm{th}}\sigma_r^2}{p_s}, & \gamma_{\mathrm{th}} > \frac{S_{\min}}{\sigma_r^2} \end{cases}$.

Proof. See Appendix D. □

D. OPS in Interference-limited Environment

In the considered DF FDR network, the relay may suffer severe RSI from its own transmit signal due to inefficient IC processing. Experiments have shown that RSI contains a strong specular component such that the RSI channel can be modeled as Rician [24] and this fading feature has been widely adopted in recent studies [28], [37]. In such cases, it is reasonable to assume that the received RSI power is relatively higher than the noise power at the relay.

Similarly to the approximation in (20), the noise power is negligible in the interference-limited environment, so that the SINR at the relay is approximated as

$$\gamma_r \approx \frac{1-\eta\rho g_a}{\eta\rho g_b}, \quad (29)$$

whereas γ_d is still given by (11). Differently from an FDR node that has a stable power supply, the considered FDR node has to harvest energy from the ambient RF signal. The corresponding interference-limited scenario results from not only a strong RSI channel gain, but also a sufficient amount of the harvested energy or equivalently an enough high p_r, which requires that $\tilde{p}_s > S_{\min}$. Therefore, in the interference-limited environment, we can assume that the event $\tilde{p}_s > S_{\min}$ occurs with a probability 1 and an outage event happens only when $\gamma < \gamma_{\mathrm{th}}$.

Proposition 6. *In the interference-limited environment, the end-to-end outage probability achieved by PS-SWIPT in the DF FDR network is given by*

$$P_{\mathrm{out}}^{\mathrm{I}} = 1 - I_1^{\infty} I_2, \quad (30)$$

where I_1^{∞} *is given by* (19) *and* I_2 *is given by* (14b).

Proof. By substituting (29) and $0 < g_b \le g_a < 1$ into the term $\Pr\{\gamma_r > \gamma_{\mathrm{th}}\}$, it can be shown that $\Pr\{\gamma_r > \gamma_{\mathrm{th}}\} = I_1^{\infty}$, where I_1^{∞} is given by (19). Then, by applying (A.1) and I_2 of Proposition 1, we arrive at (30). □

When $p_s \to \infty$, we have $I_2 = 1$ and hence, the performance floor of (30) is given by $P_{\mathrm{out}}^{\mathrm{I}} = 1 - I_1^{\infty}$, which converges to that of (18).

Proposition 7. *In the interference-limited environment, the OPS ratio* ρ^* *that maximizes the end-to-end SINR is given by*

$$\rho^* = \frac{1}{\eta(g_a + \sqrt{p_s g_1 g_2 g_b/\sigma_d^2})} \quad (31)$$

and the corresponding end-to-end outage probability is given by

$$P_{\mathrm{out}}^{\mathrm{I}^*} = \frac{2^{2-m_1-m_2}}{\Gamma(m_1)\Gamma(m_2)} D_{m_1+m_2-1, m_1-m_2}\left(2\sqrt{\frac{g_b\sigma_d^2\gamma_{\mathrm{th}}^2}{p_s\theta_1\theta_2}}\right), \quad (32)$$

where $D_{\mu,\nu}(y) = \int_0^y x^{\mu} K_{\nu}(x)\mathrm{d}x$.

Proof. See Appendix E. □

E. Outage Probabilities of HDR-assisted PS-SWIPT

For comparison purpose, this subsection presents end-to-end outage probabilities and average throughputs achieved by PS-SWIPT in the DF HDR network.

In the DF HDR network where PS-SWIPT is employed, each block of relaying transmission is accomplished within two time phases. In the first time phase with a duration of $\frac{T}{2}$, the source transmits its signal to the relay and the relay splits the received signal for EH and ID by the ratio of $\rho : 1-\rho$. In the second time phase with a duration of $\frac{T}{2}$, the relay amplifies the received signal with the harvested energy and forwards it to the destination. The e-SINR achieved by PS-SWIPT in the DF HDR network is given by $\gamma = \min\left(\frac{(1-\rho)p_s g_1}{\sigma_r^2}, \frac{\eta\rho p_s g_1 g_2}{\sigma_d^2}\right)$. The OPS ratio ρ^* and the corresponding end-to-end outage probability for PS-SWIPT in the DF HDR network can be found in [11], where $|h_1|$ and $|h_2|$ are modeled as Rayleigh fading. By modeling $|h_1|$ and $|h_2|$ as Nakagami-m fading and considering both the EH outage and information transmission outage, the OPS ratio ρ^* that maximizes the e-SINR and the corresponding end-to-end outage probability can be respectively derived as

$$\rho^* = \frac{\sigma_d^2}{\sigma_d^2 + \eta g_2 \sigma_r^2} \quad (33)$$

and

$$P_{\mathrm{out}}^{\mathrm{HDR}} = 1 + F_{g_1}\left(\frac{\gamma_{\mathrm{th}}\sigma_r^2}{p_s}\right) - \int_{\frac{S_{\min}}{p_s}}^{\infty} f_{g_1}(x) F_{g_2}\left(\frac{(p_s x - S_{\min})\sigma_d^2}{\eta S_{\min}\sigma_r^2}\right) \mathrm{d}x + \int_{\alpha}^{\frac{\gamma_{\mathrm{th}}\sigma_r^2+S_{\min}}{p_s}} f_{g_1}(x) F_{g_2}\left(\frac{(p_s x - S_{\min})\sigma_d^2}{\eta S_{\min}\sigma_r^2}\right) \mathrm{d}x + \int_{\frac{\gamma_{\mathrm{th}}\sigma_r^2+S_{\min}}{p_s}}^{\infty} f_{g_1}(x) F_{g_2}\left(\frac{\gamma_{\mathrm{th}}\sigma_d^2}{\eta(p_s x - \gamma_{\mathrm{th}}\sigma_r^2)}\right) \mathrm{d}x, \quad (34)$$

where $\alpha = \begin{cases} \frac{S_{\min}}{p_s}, & \gamma_{\mathrm{th}} \le \frac{S_{\min}}{\sigma_r^2} \\ \frac{\gamma_{\mathrm{th}}\sigma_r^2}{p_s}, & \gamma_{\mathrm{th}} > \frac{S_{\min}}{\sigma_r^2} \end{cases}$. Comparing (33) and (34) with (25) and (26), it can be seen that the OPS ratio ρ^* and the corresponding end-to-end outage probability achieved by HDR-assisted PS-SWIPT are coincident with those of FDR-assisted PS-SWIPT in the noise-limited environment. However, since the DF HDR network accomplishes one time transmission with an effective information block of length $\frac{T}{2}$, the average throughput of the DF HDR network is given

by $C_{\rm HDR} = \frac{1}{2}(1 - P_{\rm out}^{\rm HDR})R$, where $R = \log_2(1+\gamma_{\rm th})$ is the fixed transmission rate. On the other hand, due to FDR operation, the average throughput of the DF FDR network is $C_{\rm FDR} = (1 - P_{\rm out}^{\rm FDR})R$, which is twice the average throughput of the DF HDR network when $P_{\rm out}^{\rm FDR} = P_{\rm out}^{\rm HDR}$.

III. PS-SWIPT with Energy Accumulation

In the virtual harvest-use model, the harvested energy in each block has been fully applied for relay transmission. Although the virtual harvest-use model is easy to implement, it would perform better if energy accumulation is allowed to store a part of the harvested energy for future usage. In this section, we propose a harvest-use-store model for DF FDR-assisted PS-SWIPT, which is implemented via a GS between two modes, i.e., relaying mode μ_r and harvesting mode μ_h. Note that a GS policy has been proposed for TS-based HDR transmission in [43], the GS policy applied in this study focuses on FDR transmission with PS-SWIPT.

Denoting the relay transmission power by p_r, the SINRs of the dual-hop links can be respectively written as

$$\gamma_r^{\rm GS} \triangleq \frac{(1-\rho)p_s g_1}{(1-\rho)p_r g_b + \sigma_r^2} \quad \text{and} \quad \gamma_d^{\rm GS} \triangleq \frac{p_r g_2}{\sigma_d^2}. \tag{35}$$

Then, the e-SINR of the considered DF FDR network can be expressed as $\gamma = \min\{\gamma_r^{\rm GS}, \gamma_d^{\rm GS}\}$. Since the decoding at the destination depends on whether the relay transmits or not, the relay transmission power can be expressed as

$$p_r = \begin{cases} \frac{\gamma_{\rm th}\sigma_d^2}{g_2}, & \frac{(1-\rho)p_s g_1 g_2}{(1-\rho)g_b\gamma_{\rm th}\sigma_d^2 + g_2\sigma_r^2} \geq \gamma_{\rm th} \\ \text{does not exist}, & \text{otherwise} \end{cases}, \tag{36}$$

where $\frac{(1-\rho)p_s g_1 g_2}{(1-\rho)g_b\gamma_{\rm th}\sigma_d^2 + g_2\sigma_r^2} \geq \gamma_{\rm th}$ is obtained by substituting $p_r = \frac{\gamma_{\rm th}\sigma_d^2}{g_2}$ into $\gamma_r^{\rm GS} \geq \gamma_{\rm th}$.

Without loss of generality, we assume that the odd time slot comes before the even time slot in each transmission block and the battery #1 (battery #2) tries to discharge at the odd (even) time slot. Then, we assume that the battery #1 has the size $p_b = \alpha p_s$ with $\alpha > 0$, while the size of the battery #2 is twice that of the battery #1. The battery #1 is discretized into $L+2$ energy levels $\varepsilon_i \triangleq i p_b/(L+1)$, where $i = 0, 1, \ldots, L+1$ [43], [44]. Similarly, the battery #2 is discretized into $2L+3$ energy levels, so that it has the same ε_is for $i = 0, 1, \ldots, L+1$ as those of the battery #1. We define x_i, $i = 0, 1, \ldots, L+1$ as $L+2$ energy states for the battery #1, so that the battery #1 is in state x_i when its stored energy equals to ε_i. Further, $E_0(t) \in \{\varepsilon_i : 0 \leq i \leq L+1\}$ denotes the residual energy of the battery #1 at the beginning of the t-th block. We assume that the two batteries at the relay have the same initial state. In each block, the battery #1 (battery #2) duplicates in the even (odd) slot the operational mode that is operated by the battery #2 (battery #1) in the odd (even) slot. Since the size of the battery #2 is twice that of the battery #1, the same energy state at the beginning (end) of each block for the two batteries can be ensured irrespective of the energy accumulation.

Due to PS operation and time-switching between the two batteries, the relay can simultaneously charge one battery and retransmit the decoded source signal by using the stored energy of another battery. In each transmission block, the relay can switch between two operational modes: 1) μ_h: the battery #1 (battery #2) is charged at the odd (even) time slot without discharging at the even (odd) time slot and 2) μ_r: the relay harvests energy and transmits with $\rho \in [0, 1)$. Notably, in the mode μ_r, the behavior of the relay's battery group is similar to that of the virtual harvest-use model. However, the relay transmission power p_r for the mode μ_r is supplied by the accumulated energy. Furthermore, different from $\rho \in (0, 1)$ of the virtual harvest-use model, we set $\rho \in [0, 1)$ for the mode μ_r so that the relay can transmit without power splitting (i.e., $\rho = 0$) by using its previously stored energy. In the follows, we assume the normalization of the time duration of each time slot, so that we can use energy and power interchangeably.

At the t-th block, the operational mode of the relay is denoted by $\mu(t) \in \{\mu_h, \mu_r\}$. In addition, we define two binary variables $w_1(t) \triangleq \mathbb{I}\{\mu(t) = \mu_r\}$ and $w_2(t) \triangleq \mathbb{I}\{\mu(t) = \mu_h\}$, where $\mathbb{I}$ denotes the indicator function. Based on the considered discretized battery model, the energy that can be harvested at the relay is defined as $\varepsilon_h \triangleq \varepsilon_{i_h^*}$, where

$$i_h^* = \arg \max_{i \in \{0,\ldots,L+1\}} \{\varepsilon_i : \varepsilon_i < \tilde{\varepsilon}_h\} \tag{37}$$

and

$$\tilde{\varepsilon}_h \triangleq \begin{cases} \eta_h p_s g_1, & \mu(t) = \mu_h \\ \eta_h \rho (p_s g_1 + p_r g_a), & \mu(t) = \mu_r \end{cases}. \tag{38}$$

As for the relay transmission, the relay also uses the $L+2$ discrete energy levels. Corresponding to p_r of (36), the required transmitted energy level is given by $\varepsilon_r \triangleq \varepsilon_{i_r^*}$, where

$$i_r^* = \arg \min_{i \in \{1,\ldots,L+1\}} \{\varepsilon_i : \varepsilon_i \geq \tilde{\varepsilon}_r\} \quad \text{and} \quad \tilde{\varepsilon}_r \triangleq \frac{\gamma_{\rm th}\sigma_d^2}{g_2}. \tag{39}$$

Since an outage event occurs when the source signal cannot be decoded at the destination or equivalently when the relay operates in the mode μ_h, the main optimization target is to minimize the number of times that the relay does not transmit. To this end, the GS policy prioritizes the operation mode μ_r. When the residual energy of each battery supports the required transmitted power, the GS policy switches the relay to transmission, otherwise it switches the relay to EH. At the t-th block, the GS policy can be expressed as

$$\mu^{\rm GS}(t) = \begin{cases} \mu_r, & (\gamma^{\rm GS} \geq \gamma_{\rm th}) \cap (E_0(t) \geq \tilde{\varepsilon}_r) \\ \mu_h, & ((\gamma^{\rm GS} \geq \gamma_{\rm th}) \cap (E_0(t) < \tilde{\varepsilon}_r)) \cup (\gamma^{\rm GS} < \gamma_{\rm th}) \end{cases} \tag{40}$$

and

$$E_0(t) = \min\{p_b, E_0(t-1) - w_1(t-1)\varepsilon_r + w_2(t-1)\varepsilon_h\}. \tag{41}$$

A. MC for GS Policy

The GS policy results in a specific relaying/harvesting behavior of the relay's battery group that can be represented by a finite MC and hence, the stationary distribution of this MC and the corresponding outage probability can be characterized. Without loss of generality, the battery #1 is chosen for analysis. Since the battery #1 discharges and charges at the odd and even time slots sequentially, it leads to an MC model with a two-stage state transition for each transmission block.

Assume that the initial, intermediate, and final states of the battery #1 in each transmission block are x_i, x_k, and x_j, respectively, the transitions $x_i \to x_k$ and $x_k \to x_j$ occur at the odd and even time slots, respectively, and the transition $x_i \to x_k \to x_j$ occurs throughout the whole block. Since the battery #1 tries to discharge and charge at the odd and even time slot, respectively, we have $k \le i$ and $k \le j$. Depending on whether the battery #1 discharges or not at an odd time slot, the amount of the available power for EH at the corresponding even time slot can be rewritten as

$$\tilde{\varepsilon}_h = \begin{cases} \eta_h p_s g_1, & k = i \text{ for } x_i \to x_k \to x_j \\ \eta_h \rho p_s g_1 + \eta_h \rho p_r g_a, & k < i \text{ for } x_i \to x_k \to x_j \end{cases}. \quad (42)$$

Thus, it can be shown that an outage event occurs when $k = i$ for $x_i \to x_k \to x_j$ and a non-outage event occurs when $k < i$ for $x_i \to x_k \to x_j$. For the later case, the battery #1 not only harvests energy from $\eta_h \rho p_s g_1$, but also recycles a portion of its own transmitted energy. By substituting p_r of (36) into (42), we can see that the available power for EH dependents on the link gains g_1, g_2, and g_a, which have different fading distributions. As a result, it is extremely difficult to derive the transition probabilities involving the recycled self-power term. To make the ensuing mathematical analysis tractable and to attain meaningful results, we have to omit the recycled self-power term in the following theoretical derivations. In such a case, the available power for EH can be expressed as

$$\tilde{\varepsilon}_h \approx \begin{cases} \eta_h p_s g_1, & k = i \text{ for } x_i \to x_k \to x_j \\ \eta_h \rho p_s g_1, & k < i \text{ for } x_i \to x_k \to x_j \end{cases}. \quad (43)$$

Due to the omission of the recycled self-power, strictly speaking, the ensuing theoretical analysis draws a lower bound for the end-to-end system performance of the proposed GS policy. As we can see from the numerical results lately, this approximation matches the simulation curves accurately.

Let us consider the transition matrix $\boldsymbol{P} \in \mathbb{R}^{(L+2)\times(L+2)}$ with its ith-row and jth-column element $P_{i,j}$ denoting the probability of the transition from the state x_i to the state x_j in a transmission block. Similarly, define $P_{i,k}^{\text{odd}}$ and $P_{k,j}^{\text{even}}$ as the transition probabilities at the odd and even time slots, respectively. With respect to the two-stage state transition, $P_{i,j}$ can be expressed as

$$\begin{aligned} P_{i,j} &\triangleq P_{i,i}^{\text{odd}} P_{i,j}^{\text{even}} + \sum_{k<i} P_{i,k}^{\text{odd}} P_{k,j}^{\text{even}} \\ &\triangleq \bar{P}_{i,j} + \tilde{P}_{i,j}, \end{aligned} \quad (44)$$

where $\bar{P}_{i,j} \triangleq P_{i,i}^{\text{odd}} P_{i,j}^{\text{even}}$ and $\tilde{P}_{i,j} \triangleq \sum_{k<i} P_{i,k}^{\text{odd}} P_{k,j}^{\text{even}}$ are the transition probabilities corresponding to an outage event and a non-outage event, respectively. The transition probabilities $P_{i,j}$s are discussed and determined as the follows:

1) The empty battery #1 remains empty ($x_0 \to x_0 \to x_0$): This case corresponds to an outage scenario in which the battery #1 is empty at the beginning of the odd time slot, so that $\tilde{P}_{0,0} = 0$ and $P_{0,0}^{\text{odd}} = 1$. Furthermore, at the even time slot, the amount of the available power for EH is less than ε_1, so that the battery #1 cannot charge. Then, we have $P_{0,0} = \bar{P}_{0,0} = P_{0,0}^{\text{even}}$, where $P_{0,0}^{\text{even}}$ is given by

$$P_{0,0}^{\text{even}} = \Pr\{\eta_h p_s g_1 < \varepsilon_1\} = F_{g_1}\left(\tfrac{\varepsilon_1}{\eta_h p_s}\right). \quad (45)$$

2) The empty battery #1 is partially charged ($x_0 \to x_0 \to x_j$: $0 < j < L+1$): This is the case that the battery #1 is empty at the beginning of the odd time slot and becomes partially charged at the even time slot. Since $\tilde{P}_{0,j} = 0$ and $P_{0,0}^{\text{odd}} = 1$, we have $P_{0,j} = \bar{P}_{0,j} = P_{0,j}^{\text{even}}$, where $P_{0,j}^{\text{even}}$ can be expressed as

$$\begin{aligned} P_{0,j}^{\text{even}} &= \Pr\{\varepsilon_j \le \eta_h p_s g_1 < \varepsilon_{j+1}\} \\ &= \Pr\left\{\tfrac{\varepsilon_j}{\eta_h p_s} \le g_1 < \tfrac{\varepsilon_{j+1}}{\eta_h p_s}\right\} \\ &= F_{g_1}\left(\tfrac{\varepsilon_{j+1}}{\eta_h p_s}\right) - F_{g_1}\left(\tfrac{\varepsilon_j}{\eta_h p_s}\right). \end{aligned} \quad (46)$$

3) The empty battery #1 is fully charged ($x_0 \to x_0 \to x_{L+1}$): This is the case that the empty battery #1 becomes fully charged at the end of the even time slot. Since $\tilde{P}_{0,L+1} = 0$ and $P_{0,0}^{\text{odd}} = 1$, we have $P_{0,L+1} = \bar{P}_{0,L+1} = P_{0,L+1}^{\text{even}}$, where $P_{0,L+1}^{\text{even}}$ is given by

$$P_{0,L+1}^{\text{even}} = \Pr\{\eta_h p_s g_1 \ge p_b\} = \bar{F}_{g_1}\left(\tfrac{p_b}{\eta_h p_s}\right). \quad (47)$$

4) The non-empty battery #1 is fully charged ($x_i \to x_k \to x_{L+1}$: $0 < i \le L+1$): This is the case that the non-empty battery #1 gets fully charged at the end of the even time slot. The transition probability corresponding to an outage event is given by $\bar{P}_{i,L+1} = P_{i,i}^{\text{odd}} P_{i,L+1}^{\text{even}}$, where

$$\begin{aligned} P_{i,i}^{\text{odd}} &= \Pr\left\{((\tilde{\varepsilon}_r > \varepsilon_i) \cap (\gamma_r^{\text{GS}} \ge \gamma_{\text{th}})) \cup (\gamma_r^{\text{GS}} < \gamma_{\text{th}})\right\} \\ &= \Pr\{((g_2 < \tfrac{\gamma_{\text{th}}\sigma_d^2}{\varepsilon_i}) \cap (g_1 > \tfrac{g_b \gamma_{\text{th}}^2 \sigma_d^2}{p_s g_2} + \tfrac{\gamma_{\text{th}}\sigma_r^2}{(1-\rho)p_s})) \\ &\quad \cup (g_1 < \tfrac{g_b \gamma_{\text{th}}^2 \sigma_d^2}{p_s g_2} + \tfrac{\gamma_{\text{th}}\sigma_r^2}{(1-\rho)p_s})\} \\ &= F_{g_2}\left(\tfrac{\gamma_{\text{th}}\sigma_d^2}{\varepsilon_i}\right) \\ &\quad + \int_{\frac{\gamma_{\text{th}}\sigma_d^2}{\varepsilon_i}}^{\infty} F_{g_1}\left(\tfrac{g_b \gamma_{\text{th}}^2 \sigma_d^2}{p_s x} + \tfrac{\gamma_{\text{th}}\sigma_r^2}{(1-\rho)p_s}\right) f_{g_2}(x)\mathrm{d}x. \end{aligned} \quad (48)$$

and

$$P_{i,L+1}^{\text{even}} = \Pr\{\eta_h p_s g_1 > p_b - \varepsilon_i\} = \bar{F}_{g_1}\left(\tfrac{p_b - \varepsilon_i}{\eta_h p_s}\right). \quad (49)$$

The transition probability corresponding to a non-outage event can be expressed as $\tilde{P}_{i,L+1} = \sum_{k=0}^{i-1} P_{i,k}^{\text{odd}} P_{k,L+1}^{\text{even}}$, where

$$\begin{aligned} P_{i,k}^{\text{odd}} &= \Pr\left\{((\varepsilon_i - \varepsilon_{k+1} < \tilde{\varepsilon}_r \le \varepsilon_i - \varepsilon_k) \cap (\gamma_r^{\text{GS}} \ge \gamma_{\text{th}}))\right\} \\ &= \int_{\frac{\gamma_{\text{th}}\sigma_d^2}{\varepsilon_i - \varepsilon_k}}^{\frac{\gamma_{\text{th}}\sigma_d^2}{\varepsilon_i - \varepsilon_{k+1}}} \bar{F}_{g_1}\left(\tfrac{g_b \gamma_{\text{th}}^2 \sigma_d^2}{p_s x} + \tfrac{\gamma_{\text{th}}\sigma_r^2}{(1-\rho)p_s}\right) f_{g_2}(x)\mathrm{d}x \end{aligned} \quad (50)$$

and

$$P_{k,L+1}^{\text{even}} = \Pr\{\eta_h \rho p_s g_1 > p_b - \varepsilon_k\} = \bar{F}_{g_1}\left(\tfrac{p_b - \varepsilon_k}{\eta_h \rho p_s}\right). \quad (51)$$

Then, the transition probability for this case is given by $P_{i,L+1} = \bar{P}_{i,L+1} + \tilde{P}_{i,L+1}$

5) The non-empty and non-full battery #1 remains unchanged ($x_i \to x_k \to x_i$: $0 < i < L+1$): In this case, the non-empty and non-full battery #1 has the same states at the beginning and the end of a block. The transition probability corresponding to an outage event is $\bar{P}_{i,i} = P_{i,i}^{\text{odd}} P_{i,i}^{\text{even}}$, where $P_{i,i}^{\text{odd}}$ is given by (48) and $P_{i,i}^{\text{even}} = \Pr\{\eta_h p_s g_1 < \varepsilon_1\} =$

$F_{g_1}\left(\frac{\varepsilon_1}{\eta_h p_s}\right)$. The transition probability corresponding to a non-outage event is $\tilde{P}_{i,i}=\sum_{k=0}^{i-1}P_{i,k}^{\text{odd}}P_{k,i}^{\text{even}}$, where $P_{i,k}^{\text{odd}}$ is given by (50) and

$$\begin{aligned}P_{k,i}^{\text{even}}&=\Pr\{\varepsilon_i-\varepsilon_k\le\eta_h\rho p_s g_1<\varepsilon_{i+1}-\varepsilon_k\}\\&=F_{g_1}\left(\tfrac{\varepsilon_{i+1}-\varepsilon_k}{\eta_h\rho p_s}\right)-F_{g_1}\left(\tfrac{\varepsilon_i-\varepsilon_k}{\eta_h\rho p_s}\right).\end{aligned}\tag{52}$$

Then, the transition probability for this case can be expressed as $P_{i,i}=\bar{P}_{i,i}+\tilde{P}_{i,i}$.

6) The non-empty and non-full battery #1 is partially charged ($x_i\to x_k\to x_j$: $0<i<j<L+1$): The transition probability corresponding to an outage event is $\bar{P}_{i,j}=P_{i,i}^{\text{odd}}P_{i,i}^{\text{even}}$, where $P_{i,i}^{\text{odd}}$ is given by (48) and

$$\begin{aligned}P_{i,j}^{\text{even}}&=\Pr\{\varepsilon_j-\varepsilon_i\le\eta_h p_s g_1<\varepsilon_{j+1}-\varepsilon_i\}\\&=F_{g_1}\left(\tfrac{\varepsilon_{j+1}-\varepsilon_i}{\eta_h p_s}\right)-F_{g_1}\left(\tfrac{\varepsilon_j-\varepsilon_i}{\eta_h p_s}\right).\end{aligned}\tag{53}$$

The transition probability corresponding to a non-outage event is $\tilde{P}_{i,j}=\sum_{k=0}^{i-1}P_{i,k}^{\text{odd}}P_{k,j}^{\text{even}}$, where $P_{i,k}^{\text{odd}}$ is given by (50) and

$$\begin{aligned}P_{k,j}^{\text{even}}&=\Pr\{\varepsilon_j-\varepsilon_k\le\eta_h\rho p_s g_1<\varepsilon_{j+1}-\varepsilon_k\}\\&=F_{g_1}\left(\tfrac{\varepsilon_{j+1}-\varepsilon_k}{\eta_h\rho p_s}\right)-F_{g_1}\left(\tfrac{\varepsilon_j-\varepsilon_k}{\eta_h\rho p_s}\right).\end{aligned}\tag{54}$$

Then, the transition probability for this case can be written as $P_{i,j}=\bar{P}_{i,j}+\tilde{P}_{i,j}$.

7) The non-empty battery #1 is discharged ($x_i\to x_j$: $0\le j<i\le L+1$): In this case, the battery #1 always discharges at an odd time slot, so that $\bar{P}_{i,j}=0$. Therefore, the transition probability for this case is $P_{i,j}=\tilde{P}_{i,j}=\sum_{k=0}^{j}P_{i,k}^{\text{odd}}P_{k,j}^{\text{even}}$, where $P_{i,k}^{\text{odd}}$ is given by (50) and $P_{k,j}^{\text{even}}$ is given by (54).

The stationary distribution of the battery #1's status can be denoted by $\boldsymbol{\pi}\triangleq[\pi_0,\pi_1,\ldots,\pi_{L+1}]^T\in\mathbb{R}^{L+2}$, where π_i, $i\in\{0,1,\ldots,L+1\}$ represents the stationary probability of the residual energy level at the battery #1 being ε_i. By using the similar methods in [43], we can verify that the transition matrix $\boldsymbol{P}$ is irreducible and row stochastic. Thus, there must exist a unique stationary distribution $\boldsymbol{\pi}$ that satisfies the following equation

$$\boldsymbol{\pi}=\boldsymbol{P}^T\boldsymbol{\pi}.\tag{55}$$

By solving (55), $\boldsymbol{\pi}$ can be derived as

$$\boldsymbol{\pi}=((\boldsymbol{P}^T-\boldsymbol{I}+\boldsymbol{B})^{-1}\boldsymbol{b},\tag{56}$$

where $\boldsymbol{b}=[1,1,\ldots,1]^T\in\mathbb{R}^{L+2}$ and $\boldsymbol{B}=[\boldsymbol{b},\boldsymbol{b},\ldots,\boldsymbol{b}]\in\mathbb{R}^{(L+2)\times(L+2)}$. With respect to the two-stage state transition in each transmission block, an outage event occurs when the battery #1 does not discharge at an odd time slot, which makes the battery #1's state unchanged at that odd time slot, i.e., $k=i$ for $x_i\to x_k\to x_j$, and the corresponding transition probability is $\bar{P}_{i,j}$. Therefore, the end-to-end outage probability achieved by the GS policy can be expressed as

$$P_{\text{out}}^{\text{GS}}=\sum_{i=0}^{L+1}\pi_i\sum_{j=i}^{L+1}\bar{P}_{i,j}.\tag{57}$$

Then, the corresponding average throughput is given by

$$R^{\text{GS}}=(1-P_{\text{out}}^{\text{GS}})R.\tag{58}$$

B. Optimal (ρ^*,p_r^*)

According to (5), the available power before EH processing can be expressed as $p_h\triangleq\tilde{p}_s+p_{\text{rsi}}$. Due to path loss and power splitting, the self-power recycling results in a power loss $\Delta p_h\triangleq p_r-p_{\text{rsi}}=p_r(1-\rho g_a)$. Obviously, the optimal transmission power for the mode μ_r can be obtained from (36) as

$$p_r^*=\frac{\gamma_{\text{th}}\sigma_d^2}{g_2}\tag{59}$$

based on three facts: 1) p_r^* is the minimum transmission power that ensures successful destination decoding, 2) p_r^* renders the minimum RSI while it guarantees successful destination decoding, and 3) p_r^* renders the minimum Δp_h while it ensures successful destination decoding.

Since (59) is independent of ρ, now we can determine ρ^* with the obtained p_r^*. When the relay is allowed to transmit with p_r^*, the corresponding e-SINR can be expressed as

$$\gamma=\min\left\{\gamma_r^{\text{GS}},\gamma_{\text{th}}\right\},\tag{60}$$

where the received SINR at the relay becomes $\gamma_r^{\text{GS}}=\frac{(1-\rho)p_s g_1 g_2}{(1-\rho)g_b\gamma_{\text{th}}\sigma_d^2+g_2\sigma_r^2}$. For the mode μ_r, the available power for EH can be rewritten as $p_h=\tilde{p}_s+\frac{\rho\gamma_{\text{th}}\sigma_d^2 g_a}{g_2}$. Since p_h (or γ_r^{GS}) is monotonically increasing (or decreasing) with respect to $\rho\in[0,1)$, we should set ρ as large as possible to harvest the allowed maximum energy, meanwhile keep γ_r^{GS} to be no less than γ_{th} to guarantee successful decoding at the relay. Therefore, the optimal ρ^* for the mode μ_r that ensures successful decoding at the relay and harvests energy as much as possible is obtained by solving $\gamma_r^{\text{GS}}=\gamma_{\text{th}}$. For the mode μ_h, we always have $\rho=1$. Thus, mathematically speaking, the optimal ρ^* can be expressed as

$$\rho^*=\begin{cases}1-\frac{g_2\gamma_{\text{th}}\sigma_r^2}{p_s g_1 g_2-g_b\gamma_{\text{th}}^2\sigma_d^2}, & \mu(t)=\mu_r\\ 1, & \mu(t)=\mu_h\end{cases}.\tag{61}$$

Note that $\frac{(1-\rho)p_s g_1 g_2}{(1-\rho)g_b\gamma_{\text{th}}\sigma_d^2+g_2\sigma_r^2}\ge\gamma_{\text{th}}$ in (36) guarantees that $\rho^*\in[0,1)$ for the mode μ_r. Further, when the RSI in the baseband is eliminated sufficiently, the optimal ρ^* can be simplified as

$$\rho^*\approx\begin{cases}1-\frac{\gamma_{\text{th}}\sigma_r^2}{p_s g_1}, & \mu(t)=\mu_r\\ 1, & \mu(t)=\mu_h\end{cases}.\tag{62}$$

By noticing the monotonicities of γ_r^{GS}, p_h, and Δp_h with respect to p_r and ρ, respectively, it is convenient to show that (ρ^*,p_r^*) is the unique global optimal point that: 1) ensures successful end-to-end transmission for the mode μ_r, 2) harvests energy as much as possible for both μ_r and μ_h, and 3) renders the minimum power loss Δp_h for the mode μ_r. Consequently, the available power for EH achieved by (ρ^*,p_r^*) can be expressed as

$$\tilde{\varepsilon}_h=\begin{cases}\eta_h p_s g_1, & k=i \text{ for } x_i\to x_k\to x_j\\ \eta_h p_s g_1-\eta_h\gamma_{\text{th}}\sigma_r^2, & k<i \text{ for } x_i\to x_k\to x_j\end{cases}.\tag{63}$$

Moreover, by employing (ρ^*,p_r^*), the mode switching criterion of the GS policy becomes

$$\mu^{\text{GS}}(t)=\begin{cases}\mu_r, & (\tilde{\gamma}_r^{\text{GS}}\ge\gamma_{\text{th}})\cap(E_0(t)\ge p_r^*)\\ \mu_h, & ((\tilde{\gamma}_r^{\text{GS}}\ge\gamma_{\text{th}})\cap(E_0(t)<p_r^*))\cup(\tilde{\gamma}_r^{\text{GS}}<\gamma_{\text{th}})\end{cases},\tag{64}$$

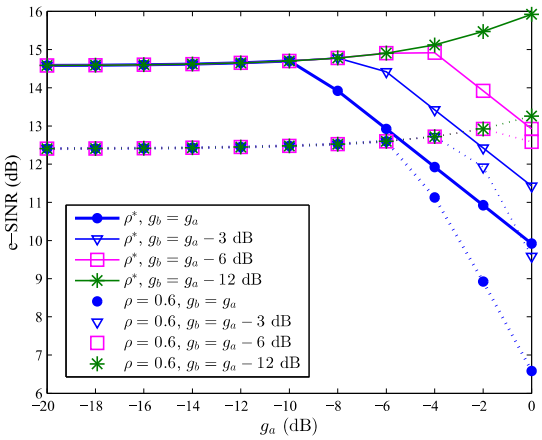

Fig. 2. e-SINR versus g_a.

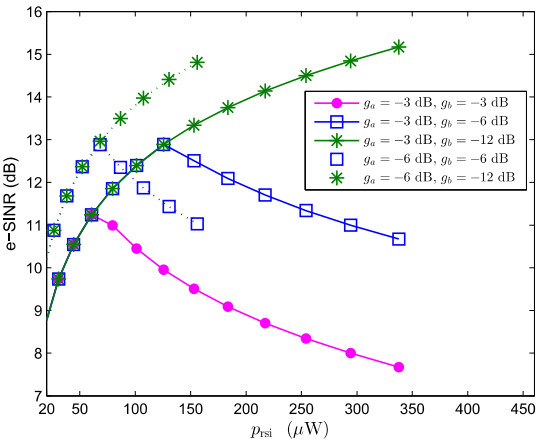

Fig. 3. Trade-off between e-SINR and $p_{\rm rsi}$.

TABLE I
SIMULATION PARAMETERS

No.	Parameter	Value
1	Carrier frequency	868 MHz
2	Bandwidth	200 kHz
3	Fixed transmission rate R	3 bps/Hz
4	$\mathcal{L}$ at $d_0 = 1$ m	-30 dB
5	Path loss exponent φ	2.5
6	Processing noise power: $\sigma^2 = \sigma_p^2 = \sigma_d^2$	-90 dBm
7	Antenna noise power σ_a^2	-100 dBm
8	Source/relay transmit antenna gain	18/8 dB

where $\tilde{\gamma}_r^{\rm GS} = \frac{p_s g_1 g_2}{g_b \gamma_{\rm th} \sigma_d^2 + g_2 \sigma_r^2}$. Then, by following the similar procedure in the previous subsection, the analytical expression of the outage probability achieved by the GS policy with (ρ^*, p_r^*) can be obtained. With respect to the seven cases of $P_{i,j}$s of the MC in the previous subsection, the $P_{i,j}$s of the MC corresponding to the GS policy that employs (ρ^*, p_r^*) are provided in Appendix F.

IV. NUMERICAL RESULTS

This section presents some numerical results to validate the performance of DF FDR-assisted PS-SWIPT developed in the previous sections. In the simulations, the virtual harvest-use model and harvest-use-store model are denoted by HU and HUS models, respectively. The distances between nodes are set as $d_1 = 8$ m and $d_2 = 18$ m. The K-factor of the RSI channel in the RF-domain is set to be 30 dB [24], the energy conversion and utilization efficiencies are set as $\eta_h = 0.4$ and $\eta_t = 0.75$, respectively, and the EH receiver sensitivity is set as $\varepsilon_{\min} = -27$ dBm [39]. The size of the battery #1 is set as $p_b = m_1 \theta_1 p_s$. Considering that $\varepsilon_1 \geq \varepsilon_{\min}$ in practice, we define the actual number of the energy levels of the battery #1 by $\tilde{L} + 2$, where $\tilde{L} \triangleq \min\{L, \lfloor p_b/\varepsilon_{\min} \rfloor\}$. Unless otherwise stated, the remained parameters used in the simulations are listed in Table 1.

Fig. 2 investigates the e-SINR versus the RSI channel gain in the RF-domain for the HU model. In Fig. 2, we focus on a single block with an instantaneous channel realization: $g_1 = 2.04 \times 10^{-4}$ and $g_2 = 4.73 \times 10^{-7}$, under fading parameters: $\{m_1 = 4, m_2 = 2\}$. The source transmission power is $p_s = 30$ dBm and g_a is set to increase from -20 dB to 0 dB. As observed in Fig. 2, the proposed DF FDR-assisted PS-SWIPT with the OPS achieves the highest e-SINR in the whole g_a region. When g_a surpasses a large value, the e-SINR decreases dramatically in case that g_b remains a relatively large value. Notably, Fig. 2 shows that the decreasing g_b results in increasing e-SINR when g_a is large and the highest e-SINR is achieved with the largest g_a. This observation verifies that the RSI in the RF-domain is helpful in improving e-SINR when g_b has been reduced significantly and hence, the IC burden in the RF-domain can be alleviated.

In Fig. 3, the trade-off between the e-SINR and recycled self-power of the HU model is investigated under the same channel realization of Fig. 2. To this end, the trade-off curves are plotted by using (16) with gradually increasing ρ from 0.01 to 0.99. Notably, $p_{\rm rsi}$ is monotonically increasing with the increasing ρ. Further, the larger g_a also results in the larger $p_{\rm rsi}$. Nevertheless, when $g_b = g_a$, i.e., without active IC, the e-SINR decreases dramatically for $g_a = -3$ dB in this scenario. Fig. 3 also shows that the increasing $p_{\rm rsi}$ has the distinct effect on e-SINR with respect to different levels of RSI in the baseband. For example, when $g_a = -3$ dB and $g_b = -6$ dB, the increasing $p_{\rm rsi}$ results in an increasing e-SINR for $p_{\rm rsi} \leq 125.7$ μW, and a decreasing e-SINR for $p_{\rm rsi} > 125.7$ μW. These trade-off curves explicitly show that the increasing e-SINR requires an increasing $p_{\rm rsi}$ along with the sufficiently reduced g_b.

Fig. 4 illustrates the impact of RSI on the end-to-end outage probability of the HU model. In Fig. 4, we set $p_s = 30$ dBm and considered two sets of channel parameters: $\{m_1 = 4, m_2 = 1\}$ and $\{m_1 = 4, m_2 = 2\}$. The outage performances of the schemes of fixed ρ and ρ^* are also investigated. Fig. 4 shows that the analytical result in Proposition 1 for the scheme of fixed ρ matches well with the simulation. As a result, the outage probability achieved by DF FDR-assisted PS-SWIPT with fixed ρ is higher than that of DF FDR-assisted PS-SWIPT with ρ^*. In the low $\bar{g}_a$ region ($\bar{g}_a < -6$ dB), the outage probabilities achieved by all the schemes are constant and the outage probability achieved by DF FDR-assisted PS-SWIPT is as same as that of DF HDR-assisted PS-SWIPT. Nevertheless, the outage probability achieved by DF FDR-assisted PS-SWIPT with fixed ρ increases dramatically and approaches 1 if $\bar{g}_a$ surpasses a threshold along with a strong g_b. We observe, for the first time, that the outage probability achieved by DF FDR-assisted PS-SWIPT with ρ^* is lower than that of DF HDR-assisted PS-SWIPT for certain strong

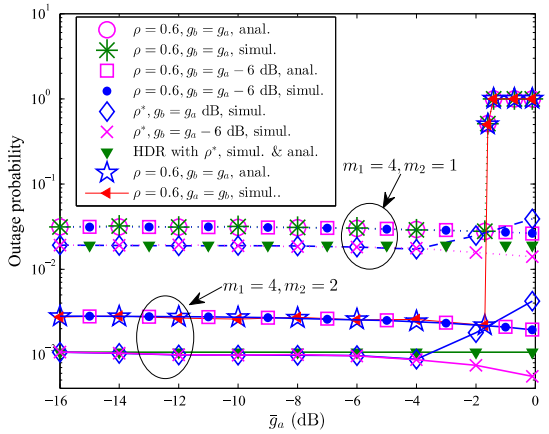

Fig. 4. Outage probability versus $\bar{g}_a$.

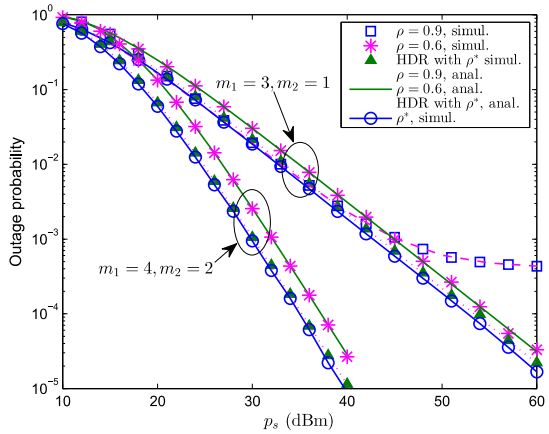

Fig. 5. Outage probability versus p_s.

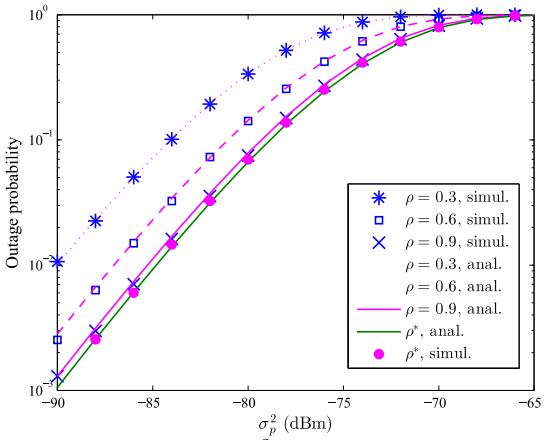

Fig. 6. Outage probability versus σ_p^2 in the noise-limited environment.

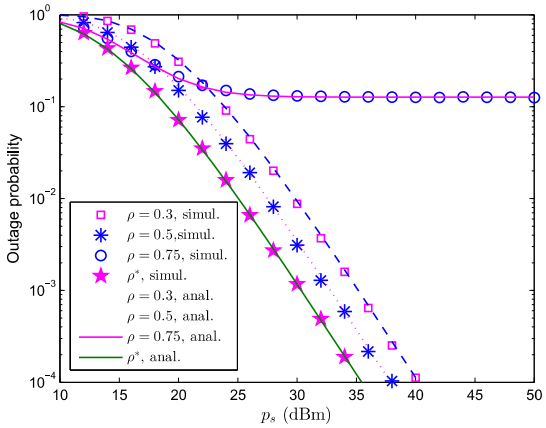

Fig. 7. Outage probability versus p_s in the interference-limited environment.

RSIs, e.g., -4 dB $< \bar{g}_a < -0.1$ dB when $p_s = 30$ dBm in this case. Notably, even when $g_b = g_a$, the outage probability achived by the scheme of ρ^* does not increases dramatically in the high g_a range. This observation also verifies that RSI can be beneficially exploited by DF FDR-assisted PS-SWIPT, whereas it has been believed that RSI is harmful in conventional FDR networks [24], [41]. Additionally, the curves in Fig. 4 verify that the approximation of $\sigma_r^2 \approx \sigma_p^2$ is accurate in analyzing the outage performance.

The end-to-end outage probability versus the source transmission power is depicted in Fig. 5, where two set of channel parameters are considered, including case 1: $\{m_1 = 3, m_2 = 1, \bar{g}_a = -1 \text{ dB}, g_b = -4\text{dB}\}$ and case 2: $\{m_1 = 4, m_2 = 2, \bar{g}_a = -6 \text{ dB}, g_b = -12\text{dB}\}$. Fig. 5 shows that the analytical and simulation results match well for the scheme with fixed ρ. The curves of the case 1 show that the outage probability for the scheme with fixed $\rho = 0.9$ is lower than that of the scheme with fixed $\rho = 0.6$ in the low p_s region. However, when the value of p_s is larger than 45 dBm, the outage probability for fixed $\rho = 0.9$ decreases very slowly and reaches an outage probability floor in the high p_s region. By substituting the corresponding parameters into (18) of Proposition 3, we have the analytical result of $P_{\text{out}}^{\infty} = 4.14 \times 10^{-4}$ for $\rho = 0.9$, which is consistent with the numerical results of Fig. 5. Fig. 5 also shows that the OPS achieves the lowest outage probability throughout the considered p_s region. Furthermore, the outage probability of the OPS is a little lower than that of DF HDR-assisted PS-SWIPT for the considered $\bar{g}_a$ and g_b. This observation also verifies that a strong RSI in the RF-domain is beneficial in decreasing the outage probability.

The end-to-end outage probability versus σ_p^2 in the noise-limited environment is examined in Fig. 6, where we set $p_s = 30$ dBm, $m_1 = 4$, $m_2 = 2$, $\bar{g}_a = -10$ dB, and $g_b = -20$ dB. Fig. 6 shows that the analytical expressions match well with the simulation results for both schemes with fixed ρ and OPS. For the scheme with fixed ρ, the outage probability decreases with increasing ρ. The reason for this phenomenon is that the channel SINRs always satisfy $\gamma_r > \gamma_d$ and a larger ρ results in a larger γ_d, so that a higher e-SINR will be obtained. The curves in Fig. 6 also verify that the smallest outage probability is achieved by the OPS in the noise-limited environment.

Fig. 7 examines the end-to-end outage probability in the interference-limited environment. In Fig. 7, the average RSI channel gains are set by $\bar{g}_a = -0.5$ dB and $g_b = -3$ dB. Further, we set $m_1 = 4$ and $m_2 = 2$. Since it has been assumed that only the passive IC is deployed in the RF-domain, it is reasonable to set $\bar{g}_a = -0.5$ dB by using antenna separation, while $\bar{g}_a = -0.5$ dB and $g_b = -3$ dB correspond to a strong RSI. Fig. 7 shows that the analytical expressions match well with the simulation results for both schemes with fixed ρ and OPS. Fig. 7 also shows that the OPS achieves the lowest outage probability. In the interference-limited environment, a relatively large ρ may lead to a relatively high RSI power and this has also been verified by Fig. 7. For fixed ρ and OPS, the outage probability decreases with increasing p_s. However, when p_s is large enough, an outage probability floor appears

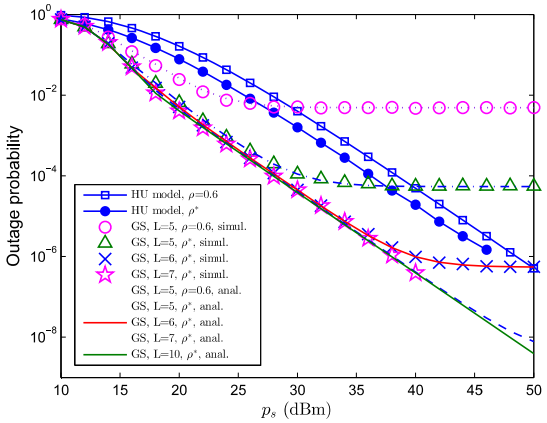

Fig. 8. Outage probability versus p_s.

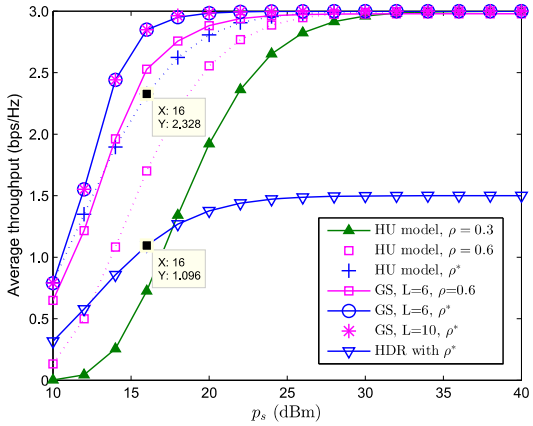

Fig. 9. Average throughput versus p_s.

due to the strong RSI resulting from a relatively larger ρ. For example, when $\rho = 0.75$, the analytical floor of (18) shows that $P_{\text{out}}^{\infty} = 1.28 \times 10^{-1}$, which is consistent with the numerical result of Fig. 7.

In Fig. 8, the outage probability versus p_s is investigated for the HUS model with the GS implementation. In the evaluation, we set $m_1 = 3$, $m_2 = 2$, $g_a = -10$ dB, and $g_b = -20$ dB. As can be seen, the GS policy achieves the smallest outage probability in the low and middle p_s regions. Further, Fig. 8 shows that the number of energy levels of the battery group is a critical parameter for the performance of the GS policy. In the low and middle p_s regions, it can be shown that the different Ls almost result in the same outage probability. Nevertheless, in the high p_s region, the outage probability achieved by the GS policy decreases with the increasing L. Moreover, the GS policy with the OPS ratio achieves a better outage performance than that of the GS policy with a fixed ρ. Additionally, the GS policy suffers from an outage floor, so that the GS policy achieves zero diversity order in the high p_s region with a limited number of energy levels. However, when L increases to 10 in this case, the same diversity as that of the HU model can be achieved by the GS policy in the high p_s region. In summary, Fig. 8 verifies that the energy accumulation and scheduling are more important than improving the instantaneous e-SINR in the low and middle p_s regions.

Fig. 9 illustrates the average throughput versus p_s. In this evaluation, we set $m_1 = 3$, $m_2 = 2$, $\bar{g}_a = -3$ dB, and $g_b = -10$ dB. As shown in Fig. 9, for all the schemes, the average throughput increases with increasing p_s. Notably, in the low p_s region, the highest average throughput is achieved by the GS policy with $L = 6$ and ρ^* for this case. Therefore, the HUS model is more suitable than the HU model for the scenario where the relay-harvested energy is small. Further, the GS policy with $L = 10$ and ρ^* achieves the same throughput as that of the GS policy with $L = 6$ and ρ^*. Hence, the requirement of a large L is not necessary for the GS policy to guarantee the achievable throughput. In the middle and high p_s regions, the throughputs achieved by the HU mode with OPS and GS policy are twice that achieved by the DF HDR-assisted PS-SWIPT with the OPS. Note that the average throughput of a conventional FDR network is at most twice that of a corresponding conventional HDR network. However, the average throughput achieved by the HU model with the OPS is slightly larger than twice that achieved by DF HDR-assisted PS-SWIPT with the OPS. For example, when $P_s = 16$ dBm, we can achieve $C_{\text{FDR}} = 2.328$ bps/Hz and $C_{\text{HDR}} = 1.096$ bps/Hz. The reason for this phenomenon is that the outage probability achieved by the HU model with the OPS is slightly smaller than that achieved by DF HDR-assisted PS-SWIPT with the OPS for certain values of g_a, as depicted in Fig. 4. Based on this observation, the IC burden in the RF-domain can be alleviated in the DF FDR network since a relatively large RSI in the RF-domain is beneficial in improving the average throughput.

V. Conclusion

This paper has investigated the virtual harvest-use model and harvest-use-store model for PS-SWIPT in a DF FDR network. With the aid of time-switched battery group for charging and discharging, the concurrent source and relay transmissions have been enabled by a PS-operated FDR node. The end-to-end outage probability achieved by DF FDR-assisted PS-SWIPT has been presented in an exact integral-form for the virtual harvest-use model. The trade-off between the e-SINR and recycled self-power has been quantified. It has also been shown that the OPS that maximizes the e-SINR can be written in closed-form using the cubic formula. The OPSs and corresponding outage probabilities in noise-limited and interference-limited environments have been respectively derived. For the harvest-use-store model, a GS policy has been applied to realize the energy accumulation. The OPS of the GS policy has been presented and the corresponding outage probability has been derived based on an MC with a two-stage state transition. The analytical and simulation results show that a relatively large RSI in the RF-domain is beneficial for increasing the recycled self-energy, so that the performances of the e-SINR and outage probability can be improved by further reducing the RSI observed in the digital-domain. The improved system performance of DF FDR-assisted PS-SWIPT over DF HDR-assisted PS-SWIPT has been verified by numerical results.

Appendix A: A proof of Proposition 1

For the DF relaying scheme, we have the expression [27], [32], [40]:

$$\begin{aligned}\Pr\{\gamma<\gamma_{\rm th}\} &= 1-\Pr\{(\gamma_r>\gamma_{\rm th})\cap(\gamma_d>\gamma_{\rm th})\}\\ &= 1-\Pr\{\gamma_r>\gamma_{\rm th}\}\Pr\{\gamma_d>\gamma_{\rm th}\}. \quad \text{(A.1)}\end{aligned}$$

In each transmission block, an outage event occurs when $\tilde{p}_s \le S_{\min}$ or when the e-SINR is less than $\gamma_{\rm th}$ given that $\tilde{p}_s > S_{\min}$. By using (A.1), the end-to-end outage probability can be evaluated as

$$\begin{aligned}P_{\rm out}^{\rm FDR} &= \Pr\{(\tilde{p}_s\le S_{\min})\cup((\tilde{p}_s>S_{\min})\cap(\gamma<\gamma_{\rm th}))\}\\ &= \Pr\{\tilde{p}_s\le S_{\min}\}+\Pr\{(\tilde{p}_s>S_{\min})\cap(\gamma<\gamma_{\rm th})\}\\ &= 1-\Pr\{(\tilde{p}_s>S_{\min})\cap(\gamma_r>\gamma_{\rm th})\cap(\gamma_d>\gamma_{\rm th})\}\\ &= 1-\Pr\left\{(g_1>\tfrac{S_{\min})}{\rho p_s})\cap(\gamma_r>\gamma_{\rm th})\cap(\gamma_d>\gamma_{\rm th})\right\}\\ &= 1-I_1I_2, \quad \text{(A.2)}\end{aligned}$$

where $I_1 \triangleq \Pr\left\{(g_1>\frac{S_{\min}}{\rho p_s})\cap(\gamma_r>\gamma_{\rm th})\right\}$ and $I_2 \triangleq \Pr\{\gamma_d>\gamma_{\rm th}\}$. In the following, the two terms I_1 and I_2 will be evaluated.

By substituting γ_r of (9) and $g_b \le g_a < 1$ into I_1, we have

$$I_1=\begin{cases}\Pr\{(g_b\le g_a<z_1(g_1))\cap(\alpha_1<g_1<\alpha_2)\cap(g_1>\alpha_3)\},\\ \Pr\{(g_b\le g_a<1)\cap(g_1>\alpha_2)\cap(g_1>\alpha_3)\},\\ \Pr\{(g_b\le g_a<z_1(g_1))\cap(g_1>\alpha_1)\cap(g_1>\alpha_3)\},\\ 0,\end{cases}$$
$$\begin{matrix}g_b\le\frac{1-\eta\rho}{\eta\rho\gamma_{\rm th}}\\ g_b\le\frac{1-\eta\rho}{\eta\rho\gamma_{\rm th}}\\ \frac{1-\eta\rho}{\eta\rho\gamma_{\rm th}}<g_b\le\frac{1}{\eta\rho(\gamma_{\rm th}+1)}\\ g_b>\frac{1}{\eta\rho(\gamma_{\rm th}+1)}\end{matrix}, \quad \text{(A.3)}$$

where $\alpha_1\triangleq\frac{(1-\eta\rho g_b)\gamma_{\rm th}\sigma_r^2}{(1-\rho)(1-\eta\rho g_b(\gamma_{\rm th}+1))p_s}$, $\alpha_2\triangleq\frac{(1-\eta\rho)\gamma_{\rm th}\sigma_r^2}{(1-\rho)(1-\eta\rho(g_b\gamma_{\rm th}+1))p_s}$, $\alpha_3 \triangleq \frac{S_{\min}}{\rho p_s}$, and $z_1(g_1) \triangleq \frac{1}{\eta\rho}-\frac{(1-\rho)p_sg_1-\gamma_{\rm th}\sigma_r^2}{(1-\rho)p_sg_1g_b\gamma_{\rm th}}$ is a function of g_1. Since $|h_a|$ has been characterized as a Rician variable, g_a follows the non-central chi-squared distribution. Denoting the Rician factor of the RSI channel by K, the CDF of g_a can be expressed as $F_{g_a}(x)=\frac{1}{\xi}(Q_1(\sqrt{2K},\sqrt{2(K+1)g_b/\bar{g}_a})-Q_1(\sqrt{2K},\sqrt{2(K+1)x/\bar{g}_a}))$, where $\xi \triangleq Q_1(\sqrt{2K},\sqrt{2(K+1)g_b/\bar{g}_a})-Q_1(\sqrt{2K},\sqrt{2(K+1)/\bar{g}_a})$ results from the truncated $g_a\in[g_b,1)$. When $g_b<\frac{1-\eta\rho}{\eta\rho\gamma_{\rm th}}$, there are three subcases in evaluating the I_1 of (A.3), i.e., 1) $\alpha_3\le\alpha_1$, 2) $\alpha_1<\alpha_3\le\alpha_2$, and 3) $\alpha_3>\alpha_2$. For the subcase of $\alpha_3<\alpha_1$ given that $g_b<\frac{1-\eta\rho}{\eta\rho\gamma_{\rm th}}$, the term I_1 can be evaluated as

$$\begin{aligned}I_1 &= \int_{\alpha_1}^{\alpha_2} f_{g_1}(x)(F_{g_a}(z_1(x))-F_{g_a}(g_b))\mathrm{d}x\\ &\quad+\int_{\alpha_2}^{\infty} f_{g_1}(x)(F_{g_a}(1)-F_{g_a}(g_b))\mathrm{d}x\\ &= \int_{\alpha_2}^{\infty} f_{g_1}(x)F_{g_a}(1)\mathrm{d}x-\int_{\alpha_1}^{\infty} f_{g_1}(x)F_{g_a}(g_b)\mathrm{d}x\\ &\quad+\int_{\alpha_1}^{\alpha_2} f_{g_1}(x)\mathrm{d}x-\tilde{I}_1(\alpha_1)\\ &= \int_{\alpha_1}^{\infty} f_{g_1}(x)\mathrm{d}x-\tilde{I}_1(\alpha_1)\\ &= \bar{F}_{g_1}(\alpha_1)-\tilde{I}_1(\alpha_1), \quad \text{(A.4)}\end{aligned}$$

where the function $\tilde{I}_1(\alpha)$ is given by

$$\tilde{I}_1(\alpha)\triangleq\frac{1}{\Gamma(m_1)\theta_1^{m_1}}\int_{\alpha}^{\alpha_2}x^{m_1-1}e^{-x/\theta_1}\bar{F}_{g_a}(z_1(x))\mathrm{d}x \quad \text{(A.5)}$$

and $\bar{F}_{g_a}(x)=\frac{1}{\xi}(Q_1(\sqrt{2K},\sqrt{2(K+1)x/\bar{g}_a})-Q_1(\sqrt{2K},\sqrt{2(K+1)/\bar{g}_a}))$ is the CCDF of g_a. In (A.4), we have applied the facts that $F_{g_a}(g_b)=0$ and $F_{g_a}(1)=1$ due to $0<g_b\le g_a<1$ in practice. Similarly, we can evaluate I_1 for the subcases of $\alpha_1<\alpha_3<\alpha_2$ and $\alpha_3>\alpha_2$ given that $g_b<\frac{1-\eta\rho}{\eta\rho\gamma_{\rm th}}$. Therefore, when $g_b<\frac{1-\eta\rho}{\eta\rho\gamma_{\rm th}}$, the term I_1 can be expressed as

$$I_1=\begin{cases}\bar{F}_{g_1}(\alpha_1)-\tilde{I}_1(\alpha_1), & \alpha_3\le\alpha_1\\ \bar{F}_{g_1}(\alpha_3)-\tilde{I}_1(\alpha_3), & \alpha_1<\alpha_3\le\alpha_2\\ \bar{F}_{g_1}(\alpha_3), & \alpha_3>\alpha_2\end{cases}. \quad \text{(A.6)}$$

Similarly to (A.6), when $\frac{1-\eta\rho}{\eta\rho\gamma_{\rm th}}<g_b<\frac{1}{\eta\rho(\gamma_{\rm th}+1)}$, the term I_1 can be evaluated as

$$I_1=\begin{cases}\bar{F}_{g_1}(\alpha_1)-\tilde{I}_2(\alpha_1), & \alpha_3\le\alpha_1\\ \bar{F}_{g_3}(\alpha_1)-\tilde{I}_2(\alpha_3), & \alpha_3>\alpha_1\end{cases}. \quad \text{(A.7)}$$

where the function $\tilde{I}_2(\alpha)$ is given by

$$\tilde{I}_2(\alpha)\triangleq\frac{1}{\Gamma(m_1)\theta_1^{m_1}}\int_{\alpha}^{\infty}x^{m_1-1}e^{-x/\theta_1}\bar{F}_{g_a}(z_1(x))\mathrm{d}x. \quad \text{(A.8)}$$

By substituting γ_d of (11) and $g_b\le g_a<1$ into I_2, we have

$$I_2=\begin{cases}\Pr\left(\frac{1-\frac{y}{\beta}}{\eta\rho}\le g_a<1\right), & (1-\eta\rho)\beta<y\le(1-\eta\rho g_b)\beta\\ 1, & y>(1-\eta\rho g_b)\beta\end{cases}, \quad \text{(A.9)}$$

where $\beta\triangleq\frac{\gamma_{\rm th}\sigma_d^2}{\eta\rho p_s\theta_1\theta_2}$, $y\triangleq x_1x_2$, and $x_i\triangleq\frac{g_i}{\theta_i}$ for $i=1$ and 2. Since x_i ($i=1$ and 2) has the standard gamma distribution, it can be shown that the PDF and CDF of y are respectively given by [45]

$$f_y(y)=\frac{2y^{\frac{1}{2}m_1+\frac{1}{2}m_2-1}}{\Gamma(m_1)\Gamma(m_2)}K_{m_1-m_2}(2\sqrt{y}) \quad \text{(A.10)}$$

and

$$F_y(y)=\frac{2^{2-m_1-m_2}}{\Gamma(m_1)\Gamma(m_2)}D_{m_1+m_2-1,m_1-m_2}(2\sqrt{y}), \quad \text{(A.11)}$$

where $D_{\mu,\nu}(y)=\int_0^y x^\mu K_\nu(x)\mathrm{d}x$. Noticing (A.10) and (A.11), (A.9) can be evaluated as

$$\begin{aligned}I_2 &= \int_{(1-\eta\rho)\beta}^{(1-\eta\rho g_b)\beta} f_y(y)\left(F_{g_a}(1)-\bar{F}_{g_a}(z_2(y))\right)\mathrm{d}y\\ &\quad+\int_{(1-\eta\rho g_b)\beta}^{\infty} f_y(y)\mathrm{d}y\\ &= \int_{(1-\eta\rho)\beta}^{\infty} f_y(y)\mathrm{d}y-\int_{(1-\eta\rho)\beta}^{(1-\eta\rho g_b)\beta} f_y(y)F_{g_a}\left(z_2(y)\right)\mathrm{d}y\\ &= \bar{F}_y(\beta)-\tilde{I}_3, \quad \text{(A.12)}\end{aligned}$$

where

$$\begin{aligned}\tilde{I}_3 &\triangleq \frac{2}{\Gamma(m_1)\Gamma(m_2)}\int_{(1-\eta\rho)\beta}^{(1-\eta\rho g_b)\beta} y^{\frac{1}{2}m_1+\frac{1}{2}m_2-1}\\ &\quad\times K_{m_1-m_2}(2\sqrt{y})F_{g_a}(z_2(y))\mathrm{d}y \quad \text{(A.13)}\end{aligned}$$

and $z_2(y)\triangleq\frac{1}{\eta\rho}(1-y/\beta)$.

APPENDIX B: A PROOF OF PROPOSITION 2

Noticing that γ_r is a monotonically decreasing function of ρ and γ_d is a monotonically increasing function of ρ, we introduce $\tilde{C}(\rho) \triangleq \gamma_r - \gamma_d$ to facilitate the determination of $\gamma = \min(\gamma_r, \gamma_d)$. Since $\frac{\partial \tilde{C}(\rho)}{\partial \rho} = -\frac{(1-\rho)^2\eta p_s^2 g_1^2 g_b + (1-\eta\rho g_a)^2 p_s g_1 \sigma_r^2}{((1-\rho)\eta\rho p_s g_1 g_b + (1-\eta\rho g_a)\sigma_r^2)^2} - \frac{\eta p_s g_1 g_2}{(1-\eta\rho g_a)^2\sigma_d^2} < 0$, $\tilde{C}(\rho)$ is a monotonically decreasing function of ρ. It can be shown that $\lim_{\rho\to 0}\tilde{C}(\rho) = \frac{p_s g_1}{\sigma_r^2} > 0$ and $\lim_{\rho\to 1}\tilde{C}(\rho) = -\frac{\eta p_s g_1 g_2}{(1-\eta g_a)\sigma_d^2} < 0$. Thus, $\tilde{C}(\rho) = 0$ has a single root in the range $(0,1)$. After some mathematical manipulations, $\tilde{C}(\rho) = 0$ can be simplified to $C(\rho) = 0$, where $C(\rho) \triangleq a_3\rho^3 + a_2\rho^2 + a_1\rho + a_0$ is a cubic function, $a_0 = -\sigma_d^2$, $a_1 = \eta(g_2\sigma_r^2 + 2g_a\sigma_d^2) + \sigma_d^2$, $a_2 = \eta^2 g_2(p_s g_1 g_b - g_a\sigma_r^2) - (1+\eta g_a)^2\sigma_d^2 + \sigma_d^2$, and $a_3 = \eta^2(g_a^2\sigma_d^2 - p_s g_1 g_2 g_b)$. By applying Ferrari's method [42], the root of $C(\rho) = 0$ in the range $(0,1)$ can be characterized by[1]

$$\rho_0 = \begin{cases} \text{the 1st root of } C(\rho)=0, & \frac{g_a^2}{g_b} > \frac{p_s g_1 g_2}{\sigma_d^2} \\ \text{the 2nd root of } C(\rho)=0, & \frac{g_a^2}{g_b} < \frac{p_s g_1 g_2}{\sigma_d^2} \end{cases}, \quad \text{(B.1)}$$

which is also the single root of $\tilde{C}(\rho) = 0$ in the range $(0,1)$. Then, it becomes convenient to find ρ^* by comparing the values of ρ and ρ_0.

When $0 < \rho \le \rho_0$, we have $\tilde{C}(\rho) \ge 0$. Therefore, the e-SINR is given by $\gamma = \gamma_d$, which is monotonically increasing with respect to ρ. Hence, the maximal e-SINR for the case of $0 < \rho \le \rho_0$ is achieved by $\rho^* = \rho_0$. When $\rho_0 \le \rho < 1$, we have $\tilde{C}(\rho) < 0$. The e-SINR becomes $\gamma = \gamma_r$ and the maximal e-SINR is achieved by $\rho^* = \rho_0$ due to the monotonically decreasing of γ_r. Therefore, the OPS ratio that achieves the maximal e-SINR is given by $\rho^* = \rho_0$.

APPENDIX C: A PROOF OF PROPOSITION 3

When the transmission power p_s goes to infinity, i.e., $p_s \to \infty$ we have $\alpha_1 \to 0$, $\alpha_2 \to 0$, $\alpha_3 \to 0$, $\beta \to 0$, and $z_1(x) \to \frac{1}{\eta\rho} - g_b\gamma_{\rm th}$. By substituting $\alpha_1 \to 0$, $\alpha_2 \to 0$, $\alpha_3 \to 0$, and $z_1(x) \to \frac{1}{\eta\rho} - g_b\gamma_{\rm th}$ into (13a), we have the following asymptotic expression:

$$I_1^{\infty} = \begin{cases} 1, & g_b \le \frac{1-\eta\rho}{\eta\rho\gamma_{\rm th}} \\ F_{g_a}\left(\frac{1}{\eta\rho} - g_b\gamma_{\rm th}\right), & \frac{1-\eta\rho}{\eta\rho\gamma_{\rm th}} < g_b \le \frac{1}{\eta\rho(\gamma_{\rm th}+1)} \\ 0, & g_b > \frac{1}{\eta\rho(\gamma_{\rm th}+1)} \end{cases}. \quad \text{(C.1)}$$

By substituting $\beta \to 0$ into (14e), we have $\tilde{I}_3 \to 0$. Furthermore, when $p_s \to \infty$, we have $\bar{F}_y(\beta) \to 1$ and hence, we arrive at $I_2 \to 1$. With all the above asymptotic expressions, it can be shown that the performance floor of the end-to-end outage probability is given by

$$P_{\rm out}^{\infty} = 1 - I_1^{\infty}. \quad \text{(C.2)}$$

[1]Since the solutions for a cubic function are extremely complicated and lengthy [42], we have omitted the closed-form expression for ρ_0 due to space limitations.

APPENDIX D: A PROOF OF PROPOSITION 5

By introducing $C(\rho) \triangleq \gamma_r - \gamma_d$, we have $\frac{\partial C(\rho)}{\partial \rho} = -\frac{p_s g_1}{\sigma_r^2} - \frac{\eta p_s g_1 g_2}{\sigma_d^2} < 0$, so that $C(\rho)$ is a monotonically decreasing function of ρ. It can be shown that $C(0) = \gamma_1 > 0$ and $C(1) = -\gamma_d < 0$ such that $C(\rho) = 0$ has a single root $\rho_0 = \frac{\sigma_d^2}{\sigma_d^2 + \eta g_2 \sigma_r^2}$ in the range $(0,1)$. When $0 < \rho \le \rho_0$, we have $C(\rho) \ge 0$. Therefore, the end-to-end SINR is given by $\gamma = \gamma_d$, which is monotonically increasing with respect to ρ. Thus, the maximal end-to-end SINR for the case of $0 < \rho \le \rho_0$ is achieved by $\rho^* = \rho_0$. When $\rho_0 \le \rho < 1$, we have $C(\rho) < 0$. The end-to-end SINR becomes $\gamma = \gamma_r$ and the maximal end-to-end SINR is achieved by $\rho^* = \rho_0$ due to the monotonic decrease of γ_r with respect to ρ. Therefore, the optimal ρ^* that achieves the maximal end-to-end SINR is $\rho^* = \rho_0 = \frac{\sigma_d^2}{\sigma_d^2 + \eta g_2 \sigma_r^2}$.

By substituting $\rho^* = \frac{\sigma_d^2}{\sigma_d^2 + \eta g_2 \sigma_r^2}$ into $\gamma = \min(\gamma_r, \gamma_d)$, the end-to-end SINR can be rewritten as $\gamma = \frac{\eta p_s g_1 g_2}{\sigma_d^2 + \eta g_2 \sigma_r^2}$. Then, the corresponding outage probability can be written as $P_{\rm out}^{\rm N*} = \Pr\{(\tilde{p}_s \le S_{\min}) \cup ((\tilde{p}_s > S_{\min}) \cap (\gamma < \gamma_{\rm th}))\} \triangleq I_3^{\rm N} + I_4^{\rm N}$, where $I_3^{\rm N} \triangleq \Pr\{(\tilde{p}_s > S_{\min}) \cap (\gamma < \gamma_{\rm th})\} = \Pr\left\{(g_2 < \frac{(p_s g_1 - S_{\min})\sigma_d^2}{\eta S_{\min}\sigma_r^2}) \cap (\gamma < \gamma_{\rm th})\right\}$ and $I_4^{\rm N} \triangleq \Pr\{\tilde{p}_s \le S_{\min}\} = \Pr\left\{g_2 \ge \frac{(p_s g_1 - S_{\min})\sigma_d^2}{\eta S_{\min}\sigma_r^2}\right\}$. The term $I_3^{\rm N}$ can be evaluated as

$$I_3^{\rm N} = \begin{cases} 1, & g_1 \le \frac{\gamma_{\rm th}\sigma_r^2}{p_s} \\ \Pr\{g_2 < \alpha_1\}, & \frac{S_{\min}}{p_s} < g_1 \le \frac{\gamma_{\rm th}\sigma_r^2 + S_{\min}}{p_s} \text{ and } \gamma_{\rm th} \le \frac{S_{\min}}{\sigma_r^2} \\ \Pr\{g_2 < \alpha_1\}, & \frac{\gamma_{\rm th}\sigma_r^2}{p_s} < g_1 \le \frac{\gamma_{\rm th}\sigma_r^2 + S_{\min}}{p_s} \text{ and } \gamma_{\rm th} > \frac{S_{\min}}{\sigma_r^2} \\ \Pr\{g_2 < \alpha_2\}, & g_1 > \frac{\gamma_{\rm th}\sigma_r^2 + S_{\min}}{p_s} \end{cases}$$

$$= F_{g_1}\left(\frac{\gamma_{\rm th}\sigma_r^2}{p_s}\right) + \int_{\alpha}^{\frac{\gamma_{\rm th}\sigma_r^2 + S_{\min}}{p_s}} f_{g_1}(x) F_{g_2}\left(\frac{(p_s x - S_{\min})\sigma_d^2}{\eta S_{\min}\sigma_r^2}\right) {\rm d}x + \int_{\frac{\gamma_{\rm th}\sigma_r^2 + S_{\min}}{p_s}}^{\infty} f_{g_1}(x) F_{g_2}\left(\frac{\gamma_{\rm th}\sigma_d^2}{\eta(p_s x - \gamma_{\rm th}\sigma_r^2)}\right) {\rm d}x, \quad \text{(D.1)}$$

where $\alpha_1 \triangleq \frac{(p_s g_1 - S_{\min})\sigma_d^2}{\eta S_{\min}\sigma_r^2}$, $\alpha_2 \triangleq \frac{\gamma_{\rm th}\sigma_d^2}{\eta(p_s g_1 - \gamma_{\rm th}\sigma_r^2)}$, and

$$\alpha = \begin{cases} \frac{S_{\min}}{p_s}, & \gamma_{\rm th} \le \frac{S_{\min}}{\sigma_r^2} \\ \frac{\gamma_{\rm th}\sigma_r^2}{p_s}, & \gamma_{\rm th} > \frac{S_{\min}}{\sigma_r^2} \end{cases}. \quad \text{(D.2)}$$

Similarly, we can evaluate $I_4^{\rm N}$ as

$$I_4^{\rm N} = 1 - \int_{\frac{S_{\min}}{p_s}}^{\infty} f_{g_1}(x) F_{g_2}\left(\frac{(p_s x - S_{\min})\sigma_d^2}{\eta S_{\min}\sigma_r^2}\right) {\rm d}x. \quad \text{(D.3)}$$

APPENDIX E: A PROOF OF PROPOSITION 7

By applying a procedure similar to that in the first part of Appendix D, it can be shown that the OPS ratio that maximizes the end-to-end SINR is given by $\rho^* = \frac{1}{\eta(g_a + \sqrt{p_s g_1 g_2 g_b/\sigma_d^2})}$. By substituting $\rho^* = \frac{1}{\eta(g_a + \sqrt{p_s g_1 g_2 g_b/\sigma_d^2})}$ into $\gamma = \min(\gamma_r, \gamma_d)$, the end-to-end SINR can be rewritten as $\gamma = \sqrt{\frac{p_s g_1 g_2}{g_b \sigma_d^2}}$. Then, the outage probability $P_{\rm out}^{\rm I} = \Pr(\gamma < \gamma_{\rm th})$ can be expressed as

$$P_{\rm out}^{\rm I} = \Pr\left(y < \frac{g_b \sigma_d^2 \gamma_{\rm th}^2}{p_s \theta_1 \theta_2}\right), \quad \text{(E.1)}$$

where $y \triangleq \frac{g_1 g_2}{\theta_1 \theta_2}$. Noticing that the CDF of y is given by $F_y(y) = \frac{2^{2-m_1-m_2}}{\Gamma(m_1)\Gamma(m_2)} D_{m_1+m_2-1, m_1-m_2}(2\sqrt{y})$, the outage probability can be evaluated as

$$P_{\text{out}}^{\text{I}} = \frac{2^{2-m_1-m_2}}{\Gamma(m_1)\Gamma(m_2)} D_{m_1+m_2-1, m_1-m_2}\left(2\sqrt{\frac{g_b \sigma_d^2 \gamma_{\text{th}}^2}{p_s \theta_1 \theta_2}}\right). \quad \text{(E.2)}$$

Appendix F: Transition Probabilities of the MC

This section presents the transition probabilities of the MC corresponding to the GS policy that employs (ρ^*, p_r^*).

The transition probabilities for the cases 1), 2), and 3) are the same as those in Subsection A of Section III. For the case 4), $\bar{P}_{i,L+1} = P_{i,i}^{\text{odd}} P_{i,L+1}^{\text{even}}$, where

$$P_{i,i}^{\text{odd}} = F_{g_2}\left(\frac{\gamma_{\text{th}}\sigma_d^2}{\varepsilon_i}\right) + \int_{\frac{\gamma_{\text{th}}\sigma_d^2}{\varepsilon_i}}^{\infty} F_{g_1}\left(\frac{g_b \gamma_{\text{th}}^2 \sigma_d^2}{p_s x} + \frac{\gamma_{\text{th}}\sigma_r^2}{p_s}\right) f_{g_2}(x) \mathrm{d}x. \quad \text{(F.1)}$$

and $P_{i,L+1}^{\text{even}}$ is the same as that of Subsection A of Section III. Furthermore, $\tilde{P}_{i,L+1} = \sum_{k=0}^{i-1} P_{i,k}^{\text{odd}} P_{k,L+1}^{\text{even}}$, where

$$P_{i,k}^{\text{odd}} = \int_{\frac{\gamma_{\text{th}}\sigma_d^2}{\varepsilon_i - \varepsilon_k}}^{\frac{\gamma_{\text{th}}\sigma_d^2}{\varepsilon_i - \varepsilon_{k+1}}} \bar{F}_{g_1}\left(\frac{g_b \gamma_{\text{th}}^2 \sigma_d^2}{p_s x} + \frac{\gamma_{\text{th}}\sigma_r^2}{p_s}\right) f_{g_2}(x) \mathrm{d}x \quad \text{(F.2)}$$

and $P_{k,L+1}^{\text{even}} = \bar{F}_{g_1}\left(\frac{p_b - \varepsilon_k + \eta_h \gamma_{\text{th}} \sigma_r^2}{\eta_h p_s}\right)$. For the case 5), $\bar{P}_{i,i}$ is the same as that of Subsection A of Section III and $\tilde{P}_{i,i} = \sum_{k=0}^{i-1} P_{i,k}^{\text{odd}} P_{k,i}^{\text{even}}$, where $P_{i,k}^{\text{odd}}$ is given by (F.2) and

$$P_{k,i}^{\text{even}} = F_{g_1}\left(\frac{\varepsilon_{i+1} - \varepsilon_k + \eta_h \gamma_{\text{th}} \sigma_r^2}{\eta_h p_s}\right) - F_{g_1}\left(\frac{\varepsilon_i - \varepsilon_k + \eta_h \gamma_{\text{th}} \sigma_r^2}{\eta_h p_s}\right). \quad \text{(F.3)}$$

For the case 6), $\bar{P}_{i,j}$ is the same as that of Subsection A of Section III and $\tilde{P}_{i,j} = \sum_{k=0}^{i-1} P_{i,k}^{\text{odd}} P_{k,j}^{\text{even}}$, where $P_{i,k}^{\text{odd}}$ is given by (F.2) and

$$P_{k,j}^{\text{even}} = F_{g_1}\left(\frac{\varepsilon_{j+1} - \varepsilon_k + \eta_h \gamma_{\text{th}} \sigma_r^2}{\eta_h p_s}\right) - F_{g_1}\left(\frac{\varepsilon_j - \varepsilon_k + \eta_h \gamma_{\text{th}} \sigma_r^2}{\eta_h p_s}\right). \quad \text{(F.4)}$$

For the case 7), $P_{i,j} = \tilde{P}_{i,j} = \sum_{k=0}^{j} P_{i,k}^{\text{odd}} P_{k,j}^{\text{even}}$, where $P_{i,k}^{\text{odd}}$ is given by (F.2) and $P_{k,j}^{\text{even}}$ is given by (F.4).

References

[1] L. R. Varshney, "Transporting information and energy simultaneously," in *Proc. IEEE Int. Symp. Inf. Theory*, Toronto, Canada, 6-11 Jul. 2008, pp. 1612–1616.

[2] P. Grover and A. Sahai, "Shannon meets Tesla: Wireless information and power transfer," in *Proc. IEEE Int. Symp. Inf. Theory*, Austin, TX, 13-18 Jun. 2010, pp. 2363–2367.

[3] X. Zhou, R. Zhang, and C. K. Ho, "Wireless information and power transfer: Architecture design and rate-energy tradeoff," *IEEE Trans. Commun.*, vol. 61, no. 11, pp. 4754–4767, Nov. 2013.

[4] R. Zhang and C. K. Ho, "MIMO broadcasting for simultaneous wireless information and power transfer," *IEEE Trans. Wireless Commun.*, vol. 12, no. 5, pp. 1989–2001, May 2013.

[5] X. Zhou, R. Zhang, and C. K. Ho, "Wireless information and power transfer in multiuser OFDM systems," *IEEE Trans. Wireless Commun.*, vol. 13, no. 4, pp. 2282–2294, Apr. 2014.

[6] F. Zhu, F. Gao, and M. Yao, "A new cognitive radio strategy for SWIPT system," in *Proc. 2014 International Workshop on High Mobility Wireless Communications*, Beijing, China, 1-3 Nov. 2014, pp. 73–77.

[7] K. Huang and V. Lau, "Enabling wireless power transfer in cellular networks: Architecture, modeling and deployment," *IEEE Trans. Wireless Commun.*, vol. 13, no. 2, pp. 902–912, Feb. 2014.

[8] S. Lohani, R. Arab Loodaricheh, E. Hossain, and V. Bhargava, "On multiuser resource allocation in relay-based wireless-powered uplink cellular networks," *IEEE Trans. Wireless Commun.*, vol. 15, no. 3, pp. 1851–1865, Mar. 2016.

[9] A. Nasir, X. Zhou, S. Durrani, and R. Kennedy, "Relaying protocols for wireless energy harvesting and information processing," *IEEE Trans. Wireless Commun.*, vol. 12, no. 7, pp. 3622–3636, Jul. 2013.

[10] ——, "Throughput and ergodic capacity of wireless energy harvesting based DF relaying network," in *Proc. IEEE Int. Conf. Commun.*, Sydney, Australia, 10-14 Jun. 2014, pp. 4066–4071.

[11] Z. Ding, S. M. Perlaza, I. Esnaola, and H. V. Poor, "Power allocation strategies in energy harvesting wireless cooperative networks," *IEEE Trans. Wireless Commun.*, vol. 13, no. 2, pp. 846–860, Feb. 2014.

[12] Z. Ding, I. Krikidis, B. Sharif, and H. V. Poor, "Wireless information and power transfer in cooperative networks with spatially random relays," *IEEE Trans. Wireless Commun.*, vol. 13, no. 8, pp. 4440–4453, Aug. 2014.

[13] H. Chen, Y. Li, Y. Jiang, Y. Ma, and B. Vucetic, "Distributed power splitting for SWIPT in relay interference channels using game theory," *IEEE Trans. Wireless Commun.*, vol. 14, no. 1, pp. 410–420, Aug. 2014.

[14] G. Zhu, C. Zhong, H. Suraweera, G. Karagiannidis, Z. Zhang, and T. Tsiftsis, "Wireless information and power transfer in relay systems with multiple antennas and interference," *IEEE Trans. Commun.*, vol. 63, no. 4, pp. 1400–1418, Apr. 2015.

[15] I. Krikidis, S. Sasaki, S. Timotheou, and Z. Ding, "A low complexity antenna switching for joint wireless information and energy transfer in MIMO relay channels," *IEEE Trans. Commun.*, vol. 62, no. 5, pp. 1577–1587, May 2014.

[16] Z. Zhou, M. Peng, Z. Zhao, and Y. Li, "Joint power splitting and antenna selection in energy harvesting relay channels," *IEEE Trans. Signal Process.*, vol. 22, no. 7, pp. 823–827, Jul. 2015.

[17] Z. Ding, C. Zhong, D. W. K. Ng, M. Peng, H. A. Suraweera, R. Schober, and H. V. Poor, "Application of smart antenna technologies in simultaneous wireless information and power transfer," *IEEE Commun. Mag.*, vol. 53, no. 4, Apr. 2015.

[18] H. Bian, Y. Fang, B. Sun, and Y. Li, "Co-time co-frequency full duplex for 802.11 WLAN," *IEEE 802.11-13/0765 r2*, Jul. 2013.

[19] M. Duarte, A. Sabharwal, V. Aggarwal, R. Jana, K. Ramakrishnan, C. Rice, and N. Shankaranarayanan, "Design and characterization of a full-duplex multiantenna system for WiFi networks," *IEEE Trans. Veh. Technol.*, vol. 63, no. 3, pp. 1160–1177, Mar. 2014.

[20] S. Hong, J. Brand, J. Choi, M. Jain, J. Mehlman, S. Katti, and P. Levis, "Applications of self-interference cancellation in 5G and beyond," *IEEE Commun. Mag.*, vol. 52, no. 2, pp. 114–121, Feb. 2014.

[21] *Text Proposal on Inband Full Duplex Relay for TR 36.814*, 3GPP, Sophia Antipolis Cedex, France, Tech. Rep. 3GPP TSG RAN WG1 R1-101659, Feb. 2010.

[22] T. Yu, S. H. Han, S. Jung, J. Son, Y. Chang, H. Kang, and R. Taori, "Proposal for full duplex relay," *Tech. Rep. IEEE C802.16j-08/106 r4*, May 2008.

[23] D. Bharadia, E. McMilin, and S. Katti, "Full duplex radios," in *Proc. 2013 ACM SIGCOMM*, Hong Kong, 12-16 Aug. 2013, pp. 375–386.

[24] M. Duarte, C. Dick, and A. Sabharwal, "Experiment-driven characterization of full-duplex wireless systems," *IEEE Trans. Wireless Commun.*, vol. 11, no. 12, pp. 4296–4307, Dec. 2012.

[25] D. Korpi, T. Riihonen, V. Syrjala, L. Anttila, M. Valkama, and R. Wichman, "Full-duplex transceiver system calculations: Analysis of ADC and linearity challenges," *IEEE Trans. Wireless Commun.*, vol. 13, no. 7, pp. 3821–3836, Jul. 2014.

[26] T. Riihonen, S. Werner, and R. Wichman, "Optimized gain control for single-frequency relaying with loop interference," *IEEE Trans. Wireless Commun.*, vol. 8, no. 6, pp. 2801–2806, Jun. 2009.

[27] H. Kim, S. Lim, H. Wang, and D. Hong, "Optimal power allocation and outage analysis for cognitive full duplex relay systems," *IEEE Trans. Wireless Commun.*, vol. 11, no. 10, pp. 3754–3765, Oct. 2012.

[28] N. Tran, L. Rodriguez, and T. Le-Ngoc, "Optimal power control and error performance for full-duplex dual-hop AF relaying under residual self-interference," *IEEE Commun. Letters*, vol. 19, no. 2, pp. 291–294, Feb. 2015.

[29] H. Suraweera, I. Krikidis, G. Zheng, C. Yuen, and P. Smith, "Low-complexity end-to-end performance optimization in MIMO full-duplex relay systems," *IEEE Trans. Wireless Commun.*, vol. 13, no. 2, pp. 913–927, Feb. 2014.

[30] I. Krikidis, H. Suraweera, P. Smith, and C. Yuen, "Full-duplex relay selection for amplify-and-forward cooperative networks," *IEEE Trans. Wireless Commun.*, vol. 11, no. 12, pp. 4381–4393, Dce. 2012.

[31] H. Cui, M. Ma, L. Song, and B. Jiao, "Relay selection for two-way full duplex relay networks with amplify-and-forward protocol," *IEEE Trans. Wireless Commun.*, vol. 13, no. 7, pp. 3768–3777, Jul. 2014.

[32] C. Zhong, H. Suraweera, G. Zheng, I. Krikidis, and Z. Zhang, "Wireless information and power transfer with full duplex relaying," *IEEE Trans. Commun.*, vol. 62, no. 10, pp. 3447–3461, Oct. 2014.
[33] M. Mohammadi, H. Suraweera, G. Zheng, C. Zhong, and I. Krikidis, "Full-duplex MIMO relaying powered by wireless energy transfer," in *Proc. 16th International Workshop on Signal Processing Advances in Wireless Communications (SPAWC)*, Stockholm, Sweden, 28 Jun.-1 Jul. 2015, pp. 296–300.
[34] Y. Zeng and R. Zhang, "Full-duplex wireless-powered relay with self-energy recycling," *IEEE Wireless Commun. Lett.*, vol. 4, no. 2, pp. 201–204, Feb. 2015.
[35] I. S. Gradshteyn and I. M. Ryzhik, *Table of Integrals, Series, and Products*. New York: Academic Press, 2007.
[36] M. K. Simon and M. S. Alouini, *Digital Communication Over Fading Channels: A Unified Approach to Performance Analysis*, 2nd ed. New York, NY: Wiley, 2005.
[37] L. Jimenez Rodriguez, N. Tran, and T. Le-Ngoc, "Performance of full-duplex AF relaying in the presence of residual self-interference," *IEEE J. Sel. Areas in Commun.*, vol. 32, no. 9, pp. 1752–1764, Sept. 2014.
[38] Y. Zeng and R. Zhang, "Optimized training design for wireless energy transfer," *IEEE Trans. Commun.*, vol. 63, no. 2, pp. 536–550, Feb. 2015.
[39] M. Stoopman, S. Keyrouz, H. J. Visser, K. Philips, and W. A. Serdijn, "Co-design of a CMOS rectifier and small loop antenna for highly sensitive RF energy harvesters," *IEEE J. Solid-State Circuits*, vol. 49, no. 3, pp. 622–634, Mar. 2014.
[40] T. Riihonen, S. Werner, and R. Wichman, "Hybrid full-duplex/half-duplex relaying with transmit power adaptation," *IEEE Trans. Wireless Commun.*, vol. 10, no. 9, pp. 3074–3085, Sept. 2011.
[41] T. Kwon, S. Lim, S. Choi, and D. Hong, "Optimal duplex mode for DF relay in terms of the outage probability," *IEEE Trans. Veh. Technol.*, vol. 59, no. 7, pp. 3628–3634, Sept. 2010.
[42] S. Neumark, *Solution of Cubic and Quartic Equations*. Oxford, NY: Pergamon Press, 1965.
[43] I. Krikidis, S. Timotheou, and S. Sasaki, "RF energy transfer for cooperative networks: Data relaying or energy harvesting?" *IEEE Commun. Letters*, vol. 16, no. 11, pp. 1772–1775, Nov. 2012.
[44] W. J. Huang, Y. W. P. Hong, and C. C. J. Kuo, "Lifetime maximization for amplify-and-forward cooperative networks," *IEEE Trans. Wireless Commun.*, vol. 7, no. 5, pp. 1800–1805, May 2008.
[45] C. S. Withers and S. Nadarajah, "On the product of gamma random variables," *Quality & Quantity*, vol. 47, no. 1, pp. 545–552, Mar. 2011.

Hongwu Liu accomplished the M.S. degree courses in Southwest Jiaotong University in 2004 and received the Ph. D. degree from Southwest Jiaotong University in 2008. During 2010-2011, he was a postdoctoral fellow at the Shanghai Institute of Microsystem and Information Technology, Chinese Academy of Science. During 2011-2013, he was a research fellow in the UWB Wireless Communications Research Center, Inha University, Korea. He is currently an associate professor at Shandong Jiaotong University. His research interests include cooperative wireless communications systems and future IoT.

Kyeong Jin Kim (SM11) received the M.S. degree from the Korea Advanced Institute of Science and Technology (KAIST) in 1991 and the M.S. and Ph.D. degrees in electrical and computer engineering from the University of California, Santa Barbara in 2000. During 1991-1995, he was a research engineer at the video research center of Daewoo Electronics, Ltd., Korea. In 1997, he joined the data transmission and networking laboratory, University of California, Santa Barbara. After receiving his degrees, he joined the Nokia research center (NRC) and Nokia Inc., Dallas, TX, as a senior research engineer, where he was, from 2005 to 2009, an L1 specialist. During 2010-2011, he was an Invited Professor at Inha University, Korea. Since 2012, he works as a senior principal research staff in the Mitsubishi Electric Research Laboratories (MERL), Cambridge, MA. His research has been focused on the transceiver design, resource management, scheduling in the cooperative wireless communications systems, cooperative spectrum sharing system, physical layer secrecy system, and device-to-device communications. Dr. Kim currently serves as an editor for the IEEE COMMUNICATIONS LETTERS and INTERNATIONAL JOURNAL OF ANTENNAS AND PROPAGATION. He also served as guest editors for the EURASIP JOURNAL ON WIRELESS COMMUNICATIONS AND NETWORKING: Special Issue on Cooperative Cognitive Networks and IET COMMUNICATIONS: Special Issue on Secure Physical Layer Communications. Since 2013, he has served as a TPC chair for the IEEE GLOBECOM Workshop on Trusted Communications with Physical Layer Security.

Kyung Sup Kwak received the Ph.D. degree from the University of California at San Diego and worked for Hughes Network Systems, and IBM Network Analysis Center, USA. Since then he has been with the School of Information and Communication Engineering, Inha University, Korea as a professor, and served the dean of the Graduate School of Information Technology and Telecommunications and the director of UWB Wireless Communications Research Center, a IT research center, Korea since 2003. In 2006, he served as the president of Korean Institute of Communication Sciences (KICS), and in 2009, the president of Korea Institute of Intelligent Transport Systems (KITS). In 1993, he received Engineering College Achievement Award from Inha University, and a service award from the Institute of Electronics Engineers of Korea (IEEK), in 1996 and 1999 he received distinguished service awards from the KICS. He received the LG Paper Award in 1998, and Motorola Paper Award in 2000. He received official commendations for UWB radio technology research and development from Minister of Information & Communication, Prime Minister, and President of Korea in 2005, 2006, and 2009, respectively. In 2007, he received Haedong Paper Award and in 2009, Haedong Scientific Award of research achievement. In 2008, he was elected for Inha Fellow Professor (IFP) and now for Inha Hanlim Fellow Professor. He published more than 200 peer-reviewed journal papers and served as TPC and Track chairs/organizing chairs for several IEEE related conferences. His research interests include multiple access communication systems, mobile & UWB radio systems, future IoT, Wireless Body Area Network: Nano Network and Molecular Communications.

H. Vincent Poor (S72, M77, SM82, F87) received the Ph.D. degree in EECS from Princeton University in 1977. From 1977 until 1990, he was on the faculty of the University of Illinois at Urbana-Champaign. Since 1990 he has been on the faculty at Princeton, where he is the Michael Henry Strater University Professor. From 2006 until 2016, he served as Dean of Princetons School of Engineering and Applied Science. He has also held visiting appointments at several universities, including most recently at Stanford and Imperial College. His research interests are in the area of wireless networks and related fields. Among his publications in these areas is the recent book Mechanisms and Games for Dynamic Spectrum Allocation (Cambridge University Press, 2014).

Dr. Poor is a Member of the National Academy of Engineering and the National Academy of Sciences, and is a Foreign Member of the Royal Society. He is also a Fellow of the American Academy of Arts and Sciences, the National Academy of Inventors, and other national and international academies. He received the Marconi and Armstrong Awards of the IEEE Communications Society in 2007 and 2009, respectively. Recent recognition of his work includes the 2014 URSI Booker Gold Medal, the 2015 EURASIP Athanasios Papoulis Award, the 2016 John Fritz Medal, and honorary doctorates from Aalborg University, Aalto University, HKUST and the University of Edinburgh.